LU-TP 22-08
February 2022

Evolutionary Properties of Neural Networks: Exploration of Robustness and Evolvability in the Genotype-Phenotype Map

Daesung Cho

Department of Astronomy and Theoretical Physics, Lund University

Master's thesis supervised by:

Jan Clemens, European Neuroscience Institute Göttingen

Victor Olariu, Lund University

LUND
UNIVERSITY

Abstract

Evolution is a fundamental and crucial part of life that hinges on two central properties: robustness and evolvability. Robustness is required to maintain essential traits despite mutations while evolvability produces novel traits that might prove beneficial in survival. While both robustness and evolvability are necessary, embracing them simultaneously seemingly leads to an inherent conflict due to their antagonistic goals driven by a shared mechanism, mutation. This conflict has been partially resolved by distinguishing phenotypic robustness and genotypic robustness. However, the general relationship between robustness and evolvability across various biological systems and how they are simultaneously facilitated are still unknown. Here, we study the relationship between robustness and evolvability of neural circuits using a genotype-phenotype map (GP map) which describes interactions between genes that ultimately determine the phenotype. We focus on canalization, the buffering of phenotypes against internal and external variations, to explain the relationship between robustness and evolvability. The pyloric circuit of the crustacean stomatogastric ganglion is used as the model system to study the relationship between robustness and evolvability. We use information theory to quantify robustness and evolvability and a novel simulation-based inference technique to examine the GP map which is used as an analog to a phenotype landscape. While robustness and evolvability are not directly correlated globally in the pyloric circuit, they are found to be linear with respect to collective traits of the pyloric rhythm as well as to individual traits. Robustness and evolvability are seen to be compromising around a region in the GP map, and we hypothesize that the pyloric rhythm is canalized, leading to local robustness and global evolvability. Multiple indicators of canalization and explicit calculation confirms that the pyloric rhythm is canalized in this neural circuit. Investigating the topology of the GP map reveals that the local landscape around the pyloric rhythm is flatter, facilitating robustness. Deviating from the canalized region leads to highly variable and steep landscape of the GP map, promoting evolvability. Gradient directions of the GP map at pyloric points are seen to be correlated, hinting at implicit mechanisms to preserve the biologically relevant behavior. In conclusion, this work demonstrates that the structure of the genotype-phenotype map in the stomatogastric ganglion facilitates robustness and evolvability through canalization. This study also establishes a scalable and generally applicable method to examine robustness and evolvability in any system involving mechanistic models.

Popular Science Description

Evolution is a vital part of life where organisms better suited to their environment survive to pass on their genes. Genes encode and largely determine how an organism ultimately develops, and thus they are considered to be the main factors of evolution. To have a better chance at survival, organisms must withstand genetic mutations to consistently produce important characteristics (robustness) such as functional legs for mobility, the correct set of organs, or the ability to communicate to fellow members in the same species. At the same time, to be able to adapt to environmental changes, they must innovate their physique or behavior (evolvability) that gives them a better chance at survival. Both robustness and evolvability stem from mutations, but their aims are contradicting. Robustness tries to maintain traits while evolvability changes them, and how biological systems promote both robustness and evolvability in general is still unknown.

This thesis studies the relationship between robustness and evolvability and the underlying mechanisms that promote these two evolutionary properties. We examine their relationship in neural circuits which are core components of many living beings that prompt behavior among many other crucial functions. As neural circuits largely determine organisms' behaviors, evolution of behavior means evolution of the neural circuit responsible for those behaviors. We use a model of a neural network responsible for controlling stomach movements in crustaceans, a group of animals that includes crabs and lobsters. This network performs its function by generating regular and stable rhythm called the pyloric rhythm and has shown robustness and potential for evolvability in previous works. Robustness and evolvability are not found to have a direct relationship in this system: they are neither opposing or supporting each other. However, we see that the pyloric rhythm produced by the circuit is canalized, meaning that this behavior is protected against small mutations.

To understand how the neural circuit canalizes the pyloric rhythm, we study how model parameters link to behavior. The structure of this transformation confirms that the underlying mechanisms of the circuit indeed canalize the pyloric rhythm. We find that this neural circuit supports robustness around the pyloric rhythm, the key biological behavior, through canalization while deviating from this behavior leads to increased evolvability. Ultimately, we show that the relationship between robustness and evolvability can be understood by studying the transformation from genetic information to the resulting traits. Additionally, this work establishes a generally applicable method that can be used to study evolutionary properties in any model at any biological scale.

Contents

List of acronyms

GP map Genotype-Phenotype Map

STG Stomatogastric Ganglion

CPG Central Pattern Generator

SNPE Sequential Neural Posterior Estimation

SBI Simulation-Based Inference

List of Figures

Chapter 1

Introduction

Evolution is a fundamental and vital process of all living organisms that reveals increasingly complex interactions and behavior with closer inspection. The wide ranges of observable characteristics from differences in physical traits to behavior even within the same taxa reveal the incredible potential and capabilities of biological systems to adapt to changing conditions [1, 2]. Biological systems impress further considering that the entirety of life is built up using a common genetic system that determines the behavioral and morphological characteristics of an individual. These traits then directly affect the likelihood of survival and the potential to produce offsprings to pass on its genetic material, leading to natural selection of advantageous traits in the given environment.

While many factors such as the physical environment can affect the final traits of an organism, the genetic information and how it is expressed largely determine the resulting traits [3]. This structure of genetic expression to traits has been studied at different scales in the form of Genotype-Phenotype Map (GP map) [3, 4]. Genotype refers to the genetic information of an organism and phenotype to the observable traits such as morphology or behavior. The GP map then is a function that transforms the genetic information to the resulting characteristics of the organism driven by interactions between genes such as epistasis and pleitropy [3]. The GP map proves to be a useful model for studying the effects of genetic interactions on the resulting traits which ultimately impacts survival fitness and evolution. In addition, the GP map can be used to study how the evolutionary capabilities of organisms evolve.

The GP map also reveals insight into the evolutionary dynamics at the population level as the structure of the map determines how genetic variability leads to phenotypic variability [3]. The influence of the GP map is evident considering the consistent characteristics of any given species despite the vast genetic diversity found in the population [1]. This phenotypic homogeneity within species confirms that the mechanisms to consistently produce crucial traits with varying genetic information are contained in the GP map. However, organisms must also be capable of producing phenotypic variability to adapt to changing environments as seen in taxonomic evolution over long time scales, also known as

macroevolution.

Macroevolutionary processes such as speciation events where a species diverges into sister species require viable mutational paths from a phenotypically homogeneous population. Since the potential mutational steps are described by the GP map, it can be used to study evolution of species over time and the underlying structure that determines their evolution. For example, punctuated equilibrium and phyletic gradualism are theories to explain taxonomic branching in evolution [5]. Punctuated equilibrium hypothesizes that observable evolution occurs in discrete time steps where a population undergoes speciation events but remains phenotypically static otherwise. On the other hand, phyletic gradualism theorizes that evolution of phynotypes is continuous and gradual, eventually transforming a species into a new distinct species. Since the GP map holistically describes mutational effects on the resulting traits, it provides a solid base to study how a population evolves over time.

1.1 Robustness and evolvability

Successful evolution requires maintenance of key traits as well as development of novel traits. These two requirements of evolution lead to central evolutionary properties, robustness and evolvability. Robustness refers to the ability to consistently generate essential phenotypes despite genotypic variation, and evolvability refers to the ability to develop novel traits that may lead to higher of survival fitness through genetic variation. The coexistence of robustness and evolvability introduces an intrinsic conflict as they aim to achieve opposing effects with a shared mechanism [6, 7]. On one hand, robustness requires phenotypic resistance to mutations while evolvability requires phenotypic variations with mutations [6]. These evolutionary properties have been examined in various models such as RNA secondary structure and Boolean models, but no direct and general relationship between them have been found [6, 7]. The potential of simultaneously promoting robustness and evolvability solely from the encoding of genetic information is limited. Therefore, there must be additional mechanisms that enable more complex genetic behaviors such as described by the GP map.

Previous work by Wagner has proposed a solution to this conflict by considering that a phenotype can be expressed by many genotypes and distinguishing robustness and evolvability of genotypes to robustness and evolvability of phenotypes [6]. He argues that a *neutral network*, a connected network of genotypes that express the same phenotype, forms a many-to-one mapping that can promote both robustness and evolvability in phenotypes. He defines genotypic robustness as the proportion of mutations from a genotype that do not lead to phenotypic changes and genotypic evolvability as the proportion of mutations that lead to phenotypic changes. Clearly, the robustness and evolvability of genotypes are antagonistic by definition. On the other hand, phenotypic robustness is defined as an average of genotypic robustness of all genotypes within the neutral network of the pheno-

type, and phenotypic evolvability is defined as the number of distinct phenotypes accessible through mutation [7].

Using a RNA model, he shows that genotype robustness and evolvability are indeed antagonistic, but phenotype robustness and evolvability can coexist and even be correlated [6]. He claims in his work that the size of the neutral network of a phenotype corresponds to the robustness of the phenotype since a larger neutral network implies a higher proportion of mutations from the network lead to the same phenotype. In addition, he argues and shows that a larger neutral network leads to higher evolvability [6, 7]. This increased evolvability stems from novel pheontypes laying at the boundaries of the neutral network. Larger neutral networks have proportionally large boundaries, ultimately resulting in higher numbers of distinct and accessible phenotypes. In this sense, populations evolve to be more robust and evolvable as it drifts around and fills out a neutral network, gaining both properties simultaneously.

This theory is illustrated in Figure 1.1 where a sizable number of connected nodes shown in c) allow robustness to mutations within the neutral network, and its extent gives access to a larger variety of phenotypes at the boundary. In contrast, a) and b) show extreme cases where mutational steps exclusively lead to the same phenotype or a different phenotype, respectively. This illustration also shows that the existence of a neutral network of a phenotype does not necessarily imply higher evolvability. The coexistence of robustness and evolvability depends heavily on the formation of the parameter space.

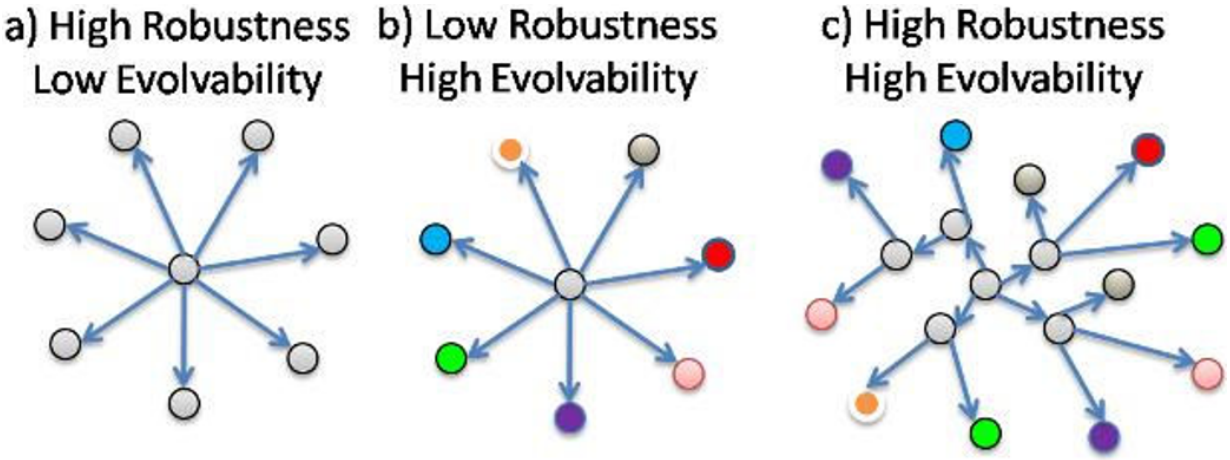

Figure 1.1: Depictions of systems with varying interactions of robustness and evolvability taken from [8]. Each node indicates a genotype that maps to some phenotype indicated by the color, and the arrows indicate an arbitrary mutation step.

In contrast to Wagner, Mayer and Hansen have argued and shown that the properties of the GP map determine the relationship between robustness and evolvability and that negative correlations between robustness and evolvability are possible [7]. Using a Boolean model they show that robustness and evolvability can be antagonistic across varying topologies of

the GP map despite distinguishing definitions of robustness and evolvability for genotypes and phenotypes as Wagner had [7]. The results of these theoretical models show that the relationship between robustness and evolvability is not universal and further reinforce the hypothesis that the mechanisms that promote both robustness and evolvability lie in the GP map.

Genotype-Phenotype Map (GP Map)

The genotype-phenotype map is a form of genetic architecture that captures genetic interactions to describe the mapping from genotype to phenotype. The GP map is relevant in many biological studies such as breeding and evolution of sex, but it is an invaluable model for understanding the evolution of evolvability and its interaction with robustness as shown by Mayer and Hansen [3, 7]. The GP map can also be thought of as a mathematical function from genotype space to phenotype space. The local topology of the GP map determines the resulting phenotypic variability, directly influencing robustness and evolvability (see Figure 1.2). A region in the GP map with a larger gradient leads to a greater phenotypic change than a region with a smaller magnitude given equally sized genotypic changes. This idea is demonstrated in Figure 1.2 in one dimension. A one-dimensional GP map cannot support both robustness and evolvability simultaneously due to dimensional limitations. However, biological genotypes and phenotypes are often multidimensional which gives the resulting multidimensional GP map in multidimensional spaces much greater flexibility to promote both robustness and evolvability simultaneously.

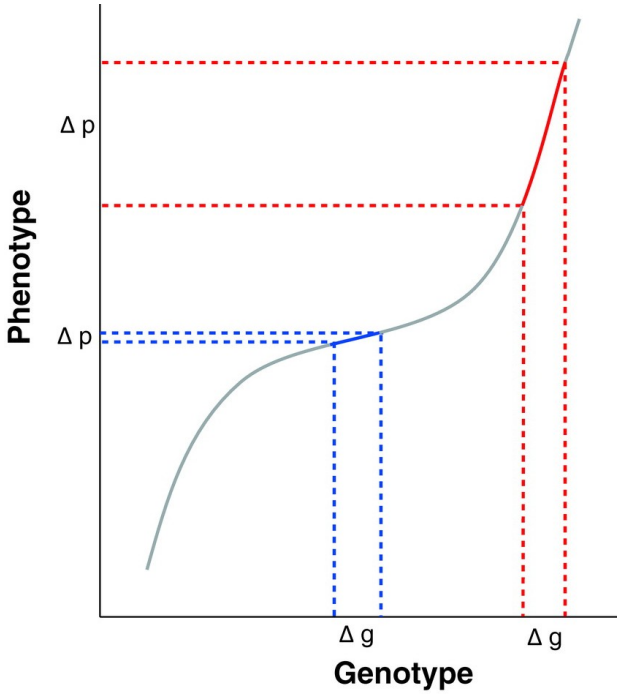

Figure 1.2: One-dimensional example of a GP map taken from [3]. Equivalent changes in genotype result in different degrees of change in the phenotype depending on the local structure.

While the one-dimensional illustration provides an intuition of the impact of the GP map, highly multi-dimensional biological systems are difficult to interpret. Thus, an additional transformation from high-dimensional phenotypic information to a scalar quantity allows easier interpretation of the GP map. This step produces a phenotype landscape given a

genotype space which can even be used to establish the survival fitness landscape since survival fitness depends on the phenotype. Treating the GP map as an analog to a phenotype landscape also allows analytic investigation of the GP map [9]. Previous work by Rice has treated the GP map as a landscape arising from a mapping function $\phi(\boldsymbol{u})$ where ϕ is some scalar quantity of phenotype and $\boldsymbol{u}$ the parameters of the phenotype [9]. Using this approach, he incorporates genetic interactions to show evolution of robustness on the mapping structure. While such analytical investigations are not done in this work, the ideas of the landscape of the GP map and its properties such as the gradient will be utilized as they tie into intuitive ideas demonstrated in Figure 1.2.

The complex evolutionary behaviors arise from the genetic interactions described by the GP map [3]. While external factors also affect the phenotype during development, this work only considers an isolated system where the phenotypic expression is driven purely by the genotype and the GP map. Possible examples of genetic interactions that can attribute to the complex behavior of robustness and evolvability include pleiotropy, epistasis, and canalization [3, 4, 8]. Pleiotropy is a phenomenon where a gene is seen to affect more than one independent trait, causing it to have a greater influence as well as greater potential for interactions. Epistasis occurs when the effect of a gene on a trait is determined by expressions of other genes. These various phenomena induce nonlinear transformations of genetic information onto phenotypes and also allow for variations of genetic architecture across species and populations [3].

GP map as a mapping structure This work treats the GP map not specifically as a mapping from genetic information to phenotype, but as a general structure that maps model parameters to the observables of the model. Hence in the context of this work, "genotype" and "model parameters" are used interchangeably as well as "phenotype" used equivalently to "behavior" or "trait." In addition, while the aforementioned genetic interactions may not apply strictly in their definitions specifically at the genetic level in this context, their respective mechanisms and effects are still useful to describe GP map in general.

Canalization

While there are varying interpretations and definitions, canalization generally refers to *phenotypic robustness against internal and external variations* [3]. The idea of canalization dates back to Waddington and the epigenetic landscape and provides an explanation for how organisms produce consistent characteristics [10]. Canalization is often depicted as rolling down the epigenetic landscape into canals where the depths of the heavily canalized grooves render small mutations inconsequential. To exit the canals and produce phenotypic change, a large perturbation is required. This concept and portrayal can also be applied to the GP map where the canalized areas form a flatter region in the phenotype landscape. This idea can be seen in Figure 1.2 where the flatter middle portion of the map can be

considered to be canalized and phenotypic variance from genotypic changes are constrained.

A corollary of canalization is that sufficiently large perturbation from a canalized state causes a diverse phenotypic expression [3]. Canalization buffers phenotypes against genotypic variance which allows a population to accumulate genetic diversity over time without harmful mutations. A large perturbation can displace the population from canalized regions in the GP map, at which point the genetic variations once suppressed by canalization are expressed. This phenomenon has been observed in various biological systems [3, 11, 12, 13]. For example, heat-shock protein Hsp90 is a "chaperone for signal-tranducing proteins," and incapacitating this protein leads to hidden variations in the signal-transduction pathway to be expressed [3]. In this case, Hsp90 behaves as a canalizing mechanism to suppress variations in the signal-transduction pathways [3]. This behavior can be seen in Figure 1.2 where the larger gradients of the GP map around a canalized region in the middle result in increased phenotypic variations.

Canalization also coincides with the hypothesis that larger neutral networks promote both robustness and evolvability. A phenotype supported by a sizable neutral network can be considered to be canalized, meaning that small mutations within the network do not affect the phenotype. However, large mutations prompt expression of phenotypes outside the neutral network as theorized by canalization. Furthermore, a population occupying an expansive neutral network (thus possessing hidden genetic variation) is prompted to express a large diversity of accessible phenotypes when greatly perturbed.

In addition to gaining access to diverse phenotypes, moving away from canalized regions tends to result in increased variability in phenotypic robustness and evolvability. As the regions of the GP map become less canalized, structural constraints that promote canalization are removed. This allows populations on the phenotype landscape to exhibit greater variety of behaviors in robustness and evolvability depending on their local topology of the GP map. There could exist small region that is lightly canalized or a large region that encourages rapid exploration of the GP map. The absence of constraints lead to increased variability in robustness and evolvability. Ultimately, the prominent indicators of canalization are:

1. phenotypic robustness to internal and external variations (only genetic variations are considered in this work)
2. increased variety of phenotypes (evolvability) away from canalized regions
3. increased variability in robustness and evolvability away from canalized regions.

1.2 Stomatogastric ganglion (STG) and the pyloric rhythm

A system that showcases the biological capacity of evolution is the nervous system and the brain which exhibit complexity in structure, behavior, and function that ranges orders of magnitudes across organisms [14]. The brain performs complex computations often involving multiple sensory inputs in short time scales and is central to the behavior and internal regulation of many organisms. In addition, neural networks at many levels are able to exhibit diverse behavior despite physical constraints and shared structures [15]. Its computational capacity, applicability, and flexibility have even inspired an extensive field of artificial neural networks where many challenging problems are tackled by leveraging the potential in the structure of the brain [16, 17].

Previous work has demonstrated computational flexibility of a cricket song recognition circuit to produce the observed range of biological phenotypes by varying physiological parameters of the neurons [15]. Crickets have also displayed high level of evolvability during speciation events where a large variety of species-specific songs are produced [15, 18, 19]. Concurrent to the behavioral flexibility and evolvability, the neural network also showcases a degree of robustness with distinct sets of parameters yielding the same behavior [15]. The degeneracy of parameter combinations that result in the same phenotype has been proposed as a mechanism for higher evolvability, and this degenerate phenomenon has been observed in many neural systems as well as biochemical networks [15, 20, 21]. While the relationship between robustness and evolvability has been studied in various systems, their behavior in neural systems remain largely unknown due to the complexity of the neural systems [6, 7, 22, 23].

The Stomatogastric Ganglion (STG) is a group of neurons that regulate the movement of the stomach in many crustaceans and has been extensively studied as central pattern generators [24, 25]. Central Pattern Generator (CPG)'s produce rhythmic patterns when active and are invaluable systems to be studied due to their functional importance, applicability to other neural systems, as well as behavioral and structural simplicity [24]. Of the two CPG's in STG, pyloric and gastric, this work studies the pyloric network and a simplified model of the pyloric circuit because this network model and its behavior have been extensively studied both biologically and mathematically. This neural circuit thus provides a solid foundation to conduct novel studies such as this. A simplified model of the pyloric circuit as well as its triphasic behavior are shown in Figure 1.3.

The essence of the STG pyloric circuit can be captured in a simple three-neuron model which only consists of two types of inhibitory connections with different time scales [20]. The three neurons in the model are the lateral pyloric (LP), pyloric (PY), and a coupling of anterior burster (AB) and pyloric dilator (PD) neurons [20]. The two types of inhibitory connections are glutamatergic and cholinergic synapses, driven by neurotransmitters glutamate and acetylcholine, respectively. Fast glutamatergic synapses exist in all three neurons

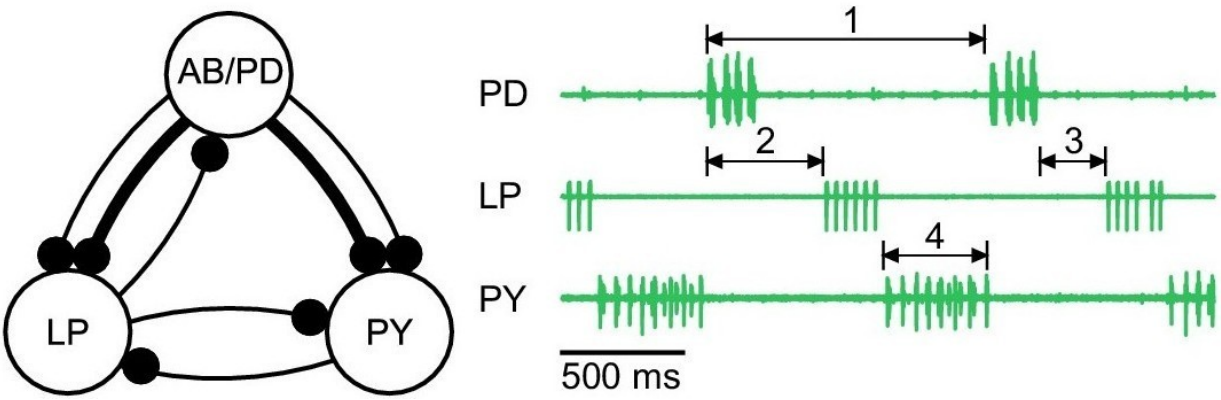

Figure 1.3: (left) A simplified three-neuron circuit diagram of the STG pyloric network and (right) the generated pyloric rhythm from extracellular recordings adapted from [17]. The thicker lines in the diagram indicate slow cholinergic connections while the thinner lines indicate faster glutamatergic connections. The numbers in the pyloric rhythm mark some of the summary features which are 1) cycle period, 2) phase delay, 3) phase gap, and 4) burst duration. Full list of features can be found in Table 1.1.

to the remaining two with the exception of PY to AB/PD. Slower cholinergic inhibitions extend from the AB/PD neuron to both the LP and PY neurons. As suggested from the number of originating inhibitions, the AB/PD neurons are critical to the stability of pattern generation and are also referred to as the pacemaker neurons [20, 25].

This neural circuit is mathematically expressed as a set of first-order ordinary differential equations [20]. Each of the neurons in the model contains eight currents: a Na^+ current, I_{NA}, a fast and a slow transient Ca^{2+} currents, I_{CaT} and I_{CaS}, a transient K^+ current, I_A, a Ca^{2+}-dependent K^+ current, $I_{K(Ca)}$, a delayed rectifier K^+ current, I_{Kd}, a hyperpolarization-activated inward current, I_H, and a leak current, I_{leak} [17, 20]. In addition, there are seven synaptic connections from the inhibitions which are described by (1.1) and (1.2) using a standard model of synaptic dynamics [26]. The synaptic current, I_s is given as

$$I_s = g_s s(V_{post} - E_s) \tag{1.1}$$

where g_s is the maximal synapse conductance, V_{post} the membrane potential of the post-synaptic neuron, and E_s the reversal potential of the synapse [20]. The evolution of the activation variable, s, is given by

$$\frac{ds}{dt} = \frac{\bar{s}(V_{pre} - s)}{\tau_s}$$
$$\bar{s}(V_{pre}) = \frac{1}{1 + \exp\frac{V_{th} - Vpre}{\delta}}; \tau_s = \frac{1 - \bar{s}(V_{pre})}{k_-} \tag{1.2}$$

where V_{pre} is the membrane potential of the presynaptic neuron, V_{th} the half-activation voltage of the synapse, δ the determining variable of the activation curve, and k_- the rate constant for transmitter-receptor dissociation rate [17, 20]. The two different types of synapses have different values for E_s and k_- but share the values for V_{th} and δ. Additional details can be found in the Methods or the following references where the model was taken [17, 20].

Robustness and evolvability in the STG pyloric circuit

Previous studies have examined the robustness of the pyloric circuit and found that disparate parameter combinations that differ by multiple orders of magnitude can produce the pyloric rhythm [20]. They show, simulating more than 20 million parameter combinations on the same neuronal model, that tightly regulated networks can exhibit functionally same behavior through compensatory mechanisms which are often found in inhibitory networks. Hence, the behavior of such networks depend not only on the parameter values but also the structure that allows interactions between the parameters as previously discussed with the GP map.

They also compared salient features of the pyloric rhythm between the model network outputs and biological data and distinguished the resulting simulation behaviors into pyloric, pyloric-like, and non-pyloric rhythms [20]. Rhythms are identified as pyloric-like if 1) the neuron bursts in every period are ordered by AB/PD-LP-PY, 2) a gap exists between AB/PD and LP bursts, and 3) LP bursts begin before PY burst and ends before PY burst ends. Pyloric rhythms in this context are a subset of pyloric-like rhythms whose features are within a range of 2 standard deviations from the mean of the biological data. The salient features and their values are shown in Table 1.1. All other behaviors such as different ordering, biphasic rhythms, or partially non-firing neurons, are considered to be non-pyloric rhythms.

Pyloric rhythms from this study were found to be rare among the simulated behaviors, but their model parameters were consistent with neuronal properties observed in biological data [20]. For example, the synaptic strength from LP to PY was narrowly defined for pyloric rhythms while the other parameters varied larger ranges. The rarity and the varieties of parameter ranges of pyloric rhythms indicate that parameters differ in importance which would be consequences of the GP map.

More recent work on the system using simulation-based inference has found distributions of parameter sets that produce pyloric rhythm [17]. The study identifies regions of parameter

Table 1.1: Salient traits of the pyloric rhythm and their experimental ranges adapted from [17, 20]. They are also used as summary statistics in SBI where the *Extracted* features were measured from the data while the *Derived* were calculated from extracted features.

	Trait	Notation	μ	σ
Extracted	Cycle period [s]	T	1.509	0.279
	AB/PD burst duration [s]	d^b_{AB}	0.582	0.133
	LP burst duration [s]	d^b_{LP}	0.399	0.113
	PY burst duration [s]	d^b_{PY}	0.530	0.150
	Gap AB/PD end to LP start [s]	Δt^{es}_{AB-LP}	0.221	0.109
	Gap LP end to PY start [s]	Δt^{es}_{LP-PY}	-0.061	0.060
	Delay AB/PD start to LP start [s]	Δt^{ss}_{AB-LP}	0.803	0.169
	Delay LP start to PY start [s]	Δt^{ss}_{LP-PY}	1.141	0.216
Derived	AB/PD duty cycle	d_{AB}	0.385	0.040
	LP duty cycle	d_{LP}	0.264	0.059
	PY duty cycle	d_{PY}	0.348	0.054
	Phase gap AB/PD end to LP start	$\Delta\phi_{AB-LP}$	0.148	0.065
	Phase gap LP end to PY start	$\Delta\phi_{LP-PY}$	-0.040	0.034
	LP start phase	ϕ_{LP}	0.533	0.054
	PY start phase	ϕ_{PY}	0.758	0.060

space with high likelihood for pyloric rhythm production using a novel technique that allows Bayesian inference of the entire 31-dimensional parameter space. They corroborate that the pyloric rhythm can be produced with disparate parameter combinations as previously shown. In addition, they show that the network behavior is maintained along a line in the region of parameter space with high likelihood for producing the pyloric rhythm despite considerable changes in parameter values.

The conserved behavior along a line in parameter space demonstrates that the behavior of the pyloric rhythm resides as a single contiguous region in the parameter space as opposed to separate clusters [17]. This structure hints at possible evolutionary paths of the circuit, but more importantly, it reveals the landscape of the GP map that allows robust conservation of behavior. The region of high likelihood can be considered to be a neutral network where internal mutations have no effect on the resulting phenotype. This idea is further reinforced by novel behaviors found within small deviations from this neutral region [17].

Previous biological studies have found variability in behavior changes from the pyloric rhythm when externally perturbed [27]. They show that the pyloric rhythm is reliably produced during tolerable temperature changes in crabs that are acclimated to different temperature ranges. The underlying states of the pyloric circuit can be seen to be adjusted according to the temperature ranges. For example, crabs that were acclimated to higher temperature ranges preserved the pyloric rhythm up to higher temperatures than crabs

that were acclimated to lower temperatures ranges. These variances hint that the neural circuits occupy different regions of the neutral space depending on the acclimatization. Furthermore, they show that the breakdown of the pyloric rhythm with sufficiently large temperature changes occurs differently for individual circuits but also for circuits acclimatized to various temperature ranges. These variances further reinforce the existence of a neutral network that expresses a qualitatively identical phenotype with a diversity of novel behavior found within small perturbations as seen in Gonçalves, *et al.* [17, 27].

Ultimately, the pyloric circuit has demonstrated its robustness and potential evolvability through its expression of the characteristic rhythm with disparate parameter combinations, tendency to localize to different regions of the neutral network depending on its environment, and novel behaviors with sufficient perturbations in both biological and computational studies. However, how these robustness and evolvability arise, the relationship between the observed robustness and potential evolvability, and the general landscape of the GP map are yet unknown. The exhibited robustness in the network, simplicity of the generated pattern, a simple mathematical model involving just three model neurons, as well as extensive biological studies make the STG an ideal model to investigate the evolutionary properties in neural systems [17].

1.3 Simulation-based inference (SBI)

High number of variables as well as observables have stunted comprehensive understanding of many mathematical models in computational neuroscience [17]. In addition, the inverse problem of fitting model parameters to biological data proves to be difficult and increasingly so with growing complexities of models and data. Commonly used methods often require accurate intuition of the model from the user and a certain amount of manual tuning of parameters to yield useful results. These methods lack the ability to be automated systematically but also inhibit holistic understanding of the parameter space that may contain more than one parameter combinations that support a given behavior [17]. Statistical inference is considered to be the traditional method for automated parameter identification in stochastic models, but it is computationally intractable for mechanistic models with dozens or even hundreds of parameters.

Bayesian inference aims to calculate the posterior over input parameters following Bayes' theorem given by

$$p(\boldsymbol{\theta}|\boldsymbol{x})p(\boldsymbol{x}) = p(\boldsymbol{x}|\boldsymbol{\theta})p(\boldsymbol{\theta}) \tag{1.3}$$

where $\boldsymbol{x}$ is some observation, $\boldsymbol{\theta}$ the input parameters, $p(\boldsymbol{\theta})$ the prior, $p(\boldsymbol{x})$ the marginal likelihood, $p(\boldsymbol{\theta}|\boldsymbol{x})$ the posterior, and $p(\boldsymbol{x}|\boldsymbol{\theta})$ the likelihood function [16]. Intuitively, the posterior describes the likelihood of some $\boldsymbol{\theta}$ given the observation $\boldsymbol{x}$. Hence, calculating the posterior is equivalent to finding model parameters, $\boldsymbol{\theta}$, that reproduce biological behavior or data, $\boldsymbol{x}$. This description of the Bayes' theorem is specified to fit the usage in this work, but the theorem can be applied generally to probabilistic events.

In the context of this work, Bayesian inference is used as a method to assess the GP map. The input variables, $\boldsymbol{\theta}$, represent the genotype or the parameters of the STG model, and the observations, $\boldsymbol{x}$, are the phenotypes, the traits of the pyloric rhythm. Finding an accurate and complete mapping from genotypes to phenotypes would require an impossible number of calculations from parameter samples covering the entire genotype space to their phenotypes. However, inferring the posterior gives a distribution of parameters that map to the given phenotype, and this method can be used to accurately characterize relevant parts of the GP map. Ultimately, Bayesian inference provides an accessible and computationally efficient method to uncover the GP map.

Obtaining the posterior requires calculation of the likelihood function, $p(\boldsymbol{x}|\boldsymbol{\theta})$, which is often intractable since it is implicit in mechanistic models [16]. The likelihood function is calculated as

$$p(\boldsymbol{x}|\boldsymbol{\theta}) = \int dz p(\boldsymbol{x}, z|\boldsymbol{\theta}) \tag{1.4}$$

where z denotes latent variables generated during model simulations and $p(\boldsymbol{x}, z|\boldsymbol{\theta})$ the joint probability density of $\boldsymbol{x}$ and z [16]. In practice, obtaining the likelihood would require integration over all possible paths within the model simulation [17]. Likelihood-free methods such as approximate Bayesian computation (ABC) that use simulations have been developed to bypass the likelihood calculation, but these traditional simulation-based methods have various limitations such as inability to handle continuous data and exponential scaling of number of required simulations with increasing data dimensions [16].

Recent developments in Simulation-Based Inference (SBI) have leveraged advances in machine learning to build a novel technique that does not require the likelihood and is generally applicable to any model with simulators [17]. Machine learning powered SBI usually achieves better accuracy, scalability, and amortization by training a deep neural network to perform density estimations [16, 17]. In this work, we use a variant of SBI called Sequential Neural Posterior Estimation (SNPE). SBI is a crucial element of the methodology, but the exact details are impertinent to the scope of this work. Hence, we briefly explain the workings, but the details can be found in the following references [17, 28, 29].

Simulation-based inference and consequently SNPE use simulations to train a deep neural network. This foundation allows the method to be flexible in its configuration, inputs, and working structure that can be better adapted to various systems [17]. The method requires three inputs: 1) a sample phenotype which can be a selection of summary features of the phenotype, 2) a mechanistic model that maps parameters $\boldsymbol{\theta}$ to some phenotype, and 3) a prior distribution $p(\boldsymbol{\theta})$. The schematic of the inference technique is shown in Figure 1.4. Given the prior distribution, a sample phenotype, and the mechanistic model, SNPE trains a conditional density estimator using a parametric model q_ϕ determined by a set of parameters, ϕ [28, 29]. The objective is to train a neural network to serve as the parametric model, q_ϕ, with weights ϕ such that $p(\boldsymbol{\theta}|\boldsymbol{x}) \approx q_\phi(\boldsymbol{\theta}|\boldsymbol{x})$. The network draws samples from the prior, $p(\boldsymbol{\theta})$, and minimizes the loss given as

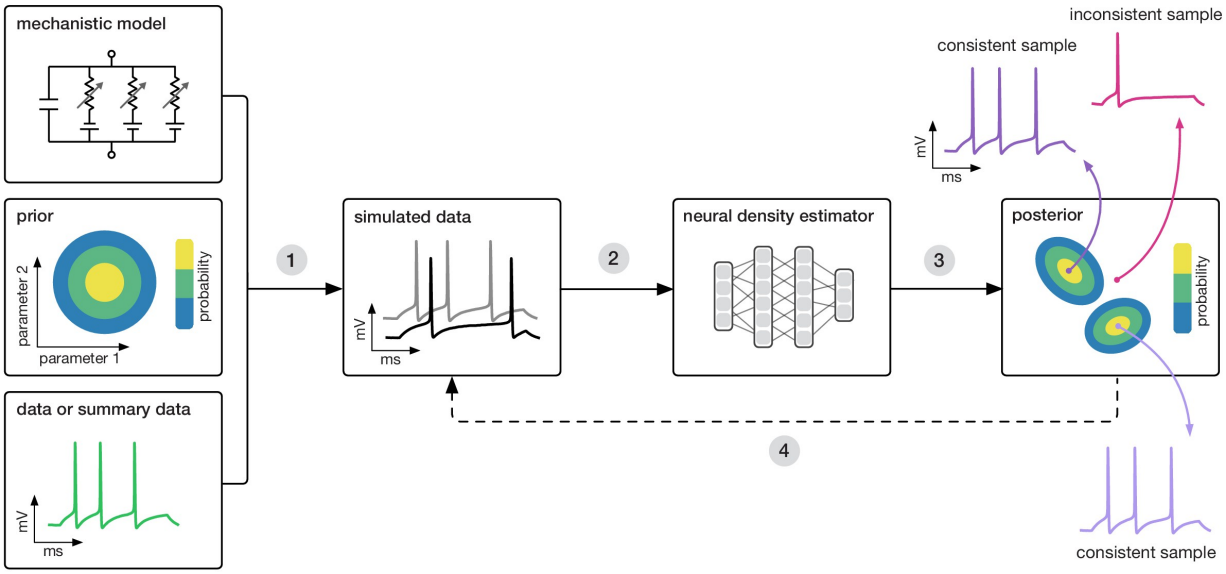

Figure 1.4: Schematic of simulation-based inference using sequential neural posterior estimation taken from [17]. Supplied with a mechanistic model, a prior distribution, and summary data ($\boldsymbol{x}$), points are sampled from the prior to simulate the model (step 1). The results are then used to train a neural density estimator (step 2) which approximates the posterior (step 3). Sequential neural posterior estimate then draws samples from the learned distribution to further train the network (step 4).

$$\mathcal{L}(\phi) = -\sum_{j=1}^{N} \log q_\phi(\boldsymbol{\theta_j}|\boldsymbol{x_j}) \tag{1.5}$$

where $\boldsymbol{\theta_j}$ and $\boldsymbol{x_j}$ are a set of parameters sampled from the prior and the resulting phenotype from the parameter set, respectively [28]. The network then learns the posterior over iterations. SNPE extends this method to allow multiple rounds of training where the parameter samples, $\boldsymbol{\theta_j}$, are not drawn from the prior but from the proposal distribution over parameters, $\tilde{p}(\theta)$, given by the conditional density estimator, q_ϕ, in the state before the round (Figure 1.4, step 4) [17]. This method of sampling enhances the learning efficiency of the network by refining the prior distribution to be more relevant for the model. This sequential neural density estimation leads to discrepancies in the resulting output, but various techniques not expanded upon here are developed to mitigate the problems [28]. Ultimately, SBI replaces likelihood calculation by training a sufficiently flexible artificial neural network, q_ϕ, that can directly estimate the posterior for large number of simulations such that $p(\boldsymbol{\theta}|\boldsymbol{x}) = q_\phi(\boldsymbol{\theta}|\boldsymbol{x})$ for $N \to \infty$ [29].

The resulting method is generally applicable to most models, can handle diverse structures and multimodal distributions, and also allows rapid amortized inference [17]. Amortized

inference allows access to the posterior distributions of any given phenotype after the initial training without requiring additional training for each new phenotype to be studied. Importantly, this feature can be used to efficiently reveal the underlying genotype network that support the supplied phenotype. As mentioned previously, the posterior distribution, a region of high likelihood of a trait, can be thought of as the neutral network of the phenotype. However, simulating the model with parameter sets from the posterior results in variations in phenotypes due to numerical variations in the continuous space. This sets the basis for further investigation into robustness and evolvability as well as the structure of the GP map.

1.4 Information theory

While robustness and evolvability have been studied previously in various systems, they still lack commonly accepted mathematical definitions that are generally applicable to any system of interest [6, 7]. In addition, robustness and evolvability have only been treated in discrete models and have never been calculated for continuous spaces. Here, robustness and evolvability are quantified using an information theoretical approach that can be adapted to any model, continuous or discrete. This measure is particularly useful as it also scales with high dimensions often found in more complex systems.

A fundamental measure of information is given by Shannon entropy, $H(X)$, given as

$$H(X) = -\sum_{i}^{N} P(x_i) \log P(x_i) \tag{1.6}$$

where $P(x_i)$ denote the probability of possible outcomes x_i from a discrete random variable X [30, 31]. While the actual value of Shannon entropy, also referred to as information entropy, has no unit, the base of the logarithmic function determines the unit of information. For example, $\log_2$ would result in information in bits while ln would result in units of *nats*.

Due to the generality of the formulation and applicability to statistical distributions in multiple dimensions, information entropy is used in many fields such as communication theory and machine learning. However, using information entropy for continuous variables introduces complications. Continuous entropy, also known as differential entropy, lacks certain compelling properties of Shannon entropy such as non-negativity and invariance under change of variables [31]. Differential entropy, $h(X)$, is given as

$$h(X) = -\int_{\chi} p(x) \log p(x) \tag{1.7}$$

where the equation differs from (1.6) only in that the integral over the support of a continuous probability distribution, χ, replaces the summation over possible outcomes. While differential entropy may lack certain desirable qualities, it still functions well as a measure

of information especially for the usage within the scope of this work. Principally, information entropy is used as a measure for robustness and evolvability as well as canalization. While there are formal differences in the formulations of entropy for discrete and continuous variables, no specific distinction is made for entropy as a measure between the two cases in this work. The distinction is omitted due to the lack of necessity from the simple usage within this scope. However, the working system is continuous, and further utilization of these entropy measures potentially requires examination into their formalities.

Entropy is a measure of uncertainty [30]. Intuitively, a probability distribution that spans a larger area in a bounded space is more uncertain than a more constrained distribution. The wider distribution with greater uncertainty thus has higher entropy than the narrower distribution. This intuition can be applied to interpretations robustness and evolvability.

Robustness and evolvability Supplied with a posterior estimate from SBI for a given phenotype, robustness can be calculated as the entropy of the posterior distribution. The shape of the distribution as well as their ranges determine the value of the entropy. Intuitively, posterior distributions of robust phenotypes will span a wider region in the parameter space and thus have higher entropy. Hence, a higher entropy indicates higher phenotypic robustness.

Evolvability is calculated as the entropy of the phenotype distribution resulting from simulating sampled points from the posterior. Larger phenotypic variation, indicating higher evolvability, results in wider distributions in the phenotype space which result in higher entropy.

Canalization Canalization can also be quantified using entropy. Often, canalization is quantified as a ratio between measures of phenotypic change and genotypic change, which lends to the idea of a measure calculated as a ratio between robustness and evolvability [32, 33]. However, as explained in Section 2.4, this work uses a fixed genotypic variation in quantifying canalization, making the robustness in the ratio constant. Hence canalization in this scope only depends on the phenotypic variability. Since the aim of canalization is to locally reduce phenotypic variability, we calculate canalization as the inverse of entropy of the phenotype distribution stemming from a fixed genotypic variation. Intuitively, this inverse entropy measure describes how tightly distributed the phenotypic variations are in relation to a fixed perturbation, directly reflecting the definition of canalization. The measures of evolvability and canalization are thus cognates in the sense that they are both calculated from phenotypic distributions. However, the origin of the genetic variation distinguishes evolvability and canalization. Genetic variation in evolvability arises from a neutral network, the posterior distribution, of a given phenotype, while genetic variation in canalization arises from a fixed perturbation.

1.5 Summary and objectives

Robustness and evolvability are seemingly conflicting properties that can be simultaneously promoted by the genetic structure and its interactions which compose a genotype-phenotype map. Consideration of a large neutral network can resolve this conflict. Most small mutations from a genotype in the neutral network will preserve the phenotype, making the phenotype robust. At the same time, a large neutral network supports evolvability since it increases the diversity of accessible phenotypes within small perturbations at the boundary of the neutral network. The pyloric circuit of the stomatogastric ganglion exhibits a robust behavior despite variations in parameters of multiple orders of magnitude through compensatory mechanisms in the circuit [17, 20, 34]. Although evolvability has never been studied explicitly for the STG, the diversity of novel behaviors found with sufficiently large perturbations from different circuit states hint at a neutral network that also supports evolvability. A novel inference method enables a systemic and holistic examination of the GP map using information entropy as a general measure of robustness, evolvability, and canalization.

Building on these foundations, this work aims to develop a framework for studying robustness and evolvability in neural networks using the STG pyloric circuit as the model system. Using novel information theoretic definitions of robustness and evolvability, the relationship between these two properties in the pyloric circuit is first studied. Specifically, robustness and evolvability of different phenotypes are quantified throughout the GP map. We use these phenotypic robustness and evolvability to study their relationship. Additionally, we study how robustness and evolvability behave with respect to individual traits of the pyloric rhythm as well as collectively. Finally, the GP map is thoroughly charted to understand the underlying structure or mechanisms that facilitate robustness and evolvability in the pyloric circuit. Canalizing behavior is specifically examined as a feature of the GP map to understand how the circuit robustly produces the pyloric rhythm.

Chapter 2

Methods

The following sections describe the methods used for two experiments which are 1) investigating robustness and evolvability in the GP map and 2) studying the structure of the GP map using fixed genetic perturbations (mutations). The first investigation is done by determining phenotypic robustness and evolvability of evenly-spaced points around the phenotype space through posterior estimation. The second study aims to unveil the structure of the GP map by mapping a wide coverage of the parameter space to the phenotype space. These approaches are prefaced by explanations of SBI usage and quantification of robustness and evolvability which are used commonly across the two studies.

2.1 Simulation-based inference and the STG network

The main purpose of SBI in this work is to predict and draw samples from the posterior distribution of the STG model. The resulting distribution is composed of parameter samples that satisfy the given model output. The samples are simply drawn by supplying a trained SBI network with a set of desired model outputs, $\boldsymbol{x}$. The resulting output distribution is a user-specified number of samples from the the posterior distribution of parameters, $p(\boldsymbol{\theta}|\boldsymbol{x})$. Each of the sampled parameter combinations theoretically map to the supplied phenotype with varying likelihood. This work largely used the computational implementation of the STG network and the SBI framework for studying this system in a previous work by Gonçalves, *et al.* [17]. The code of their implementation including the mechanistic model of the STG circuit and the usage of SBI where this work was based upon is available on `Github` [35].

STG model

The three-neuron STG model is described by the standard method of synaptic dynamics as previously mentioned [17, 20, 26]. In total, the model includes 31 parameters, of which 24 are maximal membrane conductances of each of the eight currents for the three neurons independently. The remaining 7 parameters are maximal conductances of the synapses. These 31 parameters span a 31-dimensional parameter space for the model. The synaptic conductances span uniform spaces from 0.01 nS to 1,000 nS logarithmically except the synapse from AB/PD to LP which spans from 0.01 nS to 10,000 nS [17]. The ranges of the maximal membrane conductances are shown in Table 2.1. The glutamatergic and cholinergic synapses in the model share two parameters, $V_{th} = -35$ mV and $\delta = 5$ mV [17]. The two distinct parameters, E_s and k_-, are set as -70 mV and 1/40 ms for glutamatergic synapses and -80 mV and 1/100 ms for cholinergic synapses respectively [17].

The behavior of the STG circuit is simulated as described in (1.1) and (1.2) for 10 s with a step size of 0.025 ms. The voltage traces resulting from the model were used to extract the 15 summary statistics as shown in Table 1.1 by locating spikes using a threshold. The usage of summary statistics as opposed to the entire generated data allows the network to learn more relevant features, increasing training efficiency and making the eventual interpretation easier.

Table 2.1: Ranges of the maximal membrane conductances used as parameters in the STG model. All values are in [mS cm^{-2}]. Taken from [17].

Neuron:	AB/PD		LP		PY	
Membrane	p_{low}	p_{high}	p_{low}	p_{high}	p_{low}	p_{high}
Na	0	500	0	200	0	600
CaT	0	7.5	0	2.5	0	12.5
CaS	0	8	2	12	0	4
A	0	60	10	60	30	60
KCa	0	15	0	10	0	5
Kd	25	150	0	125	50	150
H	0	0.2	0	0.06	0	0.06
Leak	0	0.01	0.01	0.04	0	0.04

The summary statistics include features that describe the rhythmic activity of all three neurons in the network: pulse period, burst durations, gaps between bursts, and delays between bursts which are extracted from the voltage traces. The remaining traits are calculated from the extracted traits. Duty cycles are found as ratios between burst durations and the cycle period of respective neurons. Phase gaps are similarly found as ratios between the respective end-to-starts and the cycle period. Start phases are ratios between start-to-starts and the cycle period.

Three features were added to the summary statistics to describe the maximal duration of each neuron with its voltage above -30 mV to distinguish traces with plateaus during the burst onset around -10 mV [17]. These features were set with a minimum of 5 ms. These features were used by Gonçalves, *et al.* to train the network, but they are omitted in our analysis as the scope of the work focuses on more biologically relevant data. Emphasis in

this work is not on the specifics of the traits but rather the general phenotypic behavior in the GP map.

Distinctions are made between pyloric and non-pyloric rhythms in this work. In this case, pyloric rhythms are behaviors whose traits are within 2σ of the experimental mean according to Table 1.1, while behaviors that do not fit into this window are considered non-pyloric. We use an extended range of phenotypes ($\mu \pm 4\sigma$) to sample points from phenotype space, and valid rhythms with traits that do not fall into $\pm 2\sigma$ of the mean are considered to be non-pyloric. In addition, *pyloric points* are used to refer to points in both phenotype space and genotype space. Pyloric points in phenotype space are defined as previously mentioned. Pyloric points in the genotype space refer to points in the 31-dimensional parameter space that maps to pyloric behavior when used in the STG model.

Simulation-based inference

This work uses an implementation of SBI called `delfi` (http://www.mackelab.org/delfi), now succeeded by `sbi` (https://www.mackelab.org/sbi). `delfi` was used to study the STG circuit in previous work by Gonçalves, *et al.*, and this work builds on the framework provided.

Training SBI requires initial training using three components: a prior distribution, a mechanistic model, and the resulting data or optionally, a user-specified summary statistics [17]. With the base configuration of SBI already given for the system from earlier work by Gonçalves, *et al.*, an instance of SBI network was trained using the same structure and parameters [17]. The implementation used SNPE-C and masked autoregressive flow for training and density estimation [17]. As with their implementation, the neural network had three layers of 100 hidden units each. This trained SBI instance was used for all further posterior sampling. The prior distribution used is a 31-dimensional uniform distribution that spans $[-\sqrt{3}, \sqrt{3}]$ in each dimension that corresponds to the 31 parameters of the STG model normalized in logarithmic space. The 15 traits as shown in Table 1.1 as well as the three additional features were used as summary statistics to train the network. The network was trained for 10 rounds and 2 epochs using 10 data points each round.

Distance measures Distances in both phenotype and genotype spaces are calculated as the Manhattan distance to mitigate the effects of higher dimensionality [36]. The Manhattan distance between two points $\boldsymbol{x}$ and $\boldsymbol{y}$ in either spaces is given by $\sum_{i=1}^{N} |x_i - y_i|$ where N is the dimensionality of the respective spaces.

However, since a reference point in the form of the natural behavior exists in the system and the posterior distribution of this phenotype can be estimated, distance in parameter space can also be calculated as the log-likelihood of a point on the posterior distribution. Using SBI, 1,000,000 samples were drawn from the posterior using the experimental mean of the

biological pyloric data as the target phenotype (see Table 1.1). The distribution was transformed to a Gaussian Kernel-Density Estimate (KDE) using `scipy.stats.gaussian_kde` with bandwidth ≈ 0.674. These distances in the parameter space were then calculated using the `logpdf` method of `gaussian_kde`. While this method is not used extensively in this work, it provides a potentially more relevant description of the parameter space especially given the high dimensionality and is used in Appendix C.

2.2 Quantification of robustness and evolvability

As mentioned in Section 1.4, robustness and evolvability are quantified using information entropy. While entropy is a useful property of probability distributions, calculation of entropy from samples drawn from non-parametric and arbitrary distributions remains a non-trivial task [31]. The posteriors generated by SBI are often such probability distributions which requires the use of non-parametric entropy estimators [17]. The entropy estimator used for this work is an implementation of the k-nearest neighbor algorithm and can be found in the following `Github` repository [37, 38]. All entropy calculations used the `get_h` function with $k = 1$ and are given in natural units, *nat*.

Entropy estimation performance Estimating entropy naturally leads to a certain level of uncertainty. Using a the covariance matrix of the posterior distribution of the pyloric rhythm, varying numbers of samples were drawn from a 31-dimensional Gaussian with the aforementioned covariance. The discrepancy between estimated entropy of the distribution and analytic entropy from the same distribution in `PyTorch` were calculated and is shown in Figure 2.1. A clear compromise between accuracy and calculation time can be seen. These measures were used along with computation times to determine samples sizes.

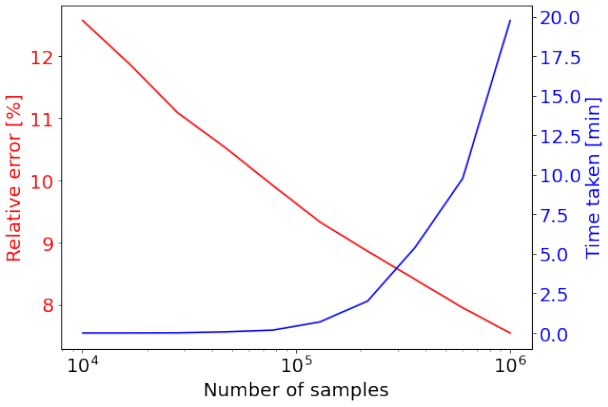

Figure 2.1: Performance of entropy estimation in accuracy (red) and estimation time (blue) with varying number of Gaussian samples. Samples were drawn from a 31-dimensional Gaussian distribution with covariance of the posterior distribution of the pyloric rhythm.

Robustness is quantified by the entropy of the posterior distribution estimated from SBI given a trait. All robustness calculations were done using 100,000 parameter samples drawn from the posterior. Evolvability is quantified as the entropy of the

distribution in phenotype space resulting from simulating the model with the sampled parameters from the posterior. The contexts where robustness and evolvability are calculated can be seen in Figure 2.2. In calculating evolvability, 50,000 points were sampled from the posterior to be simulated due to computation times in model simulation. The number of resulting points in the phenotype space varied due to a large proportion of invalid mappings. Invalid mappings arise from the network failing to produce correct rhythms, most likely due to incompatible parameter combinations [20].

Normalization Entropy is an extensive measure, whose maximum value scales with the size of the system. Robustness and evolvability correspond to the entropy of the 31-dimensional parameter space and the 15-dimensional phenotype space, respectively. To compare entropy of spaces with different dimensionalities, entropy values were divided by the maximal entropy of the respective spaces: $H^{\boldsymbol{\theta},\boldsymbol{x}}_{normalized} = \frac{H^{\boldsymbol{\theta},\boldsymbol{x}}_{i}}{H^{\boldsymbol{\theta},\boldsymbol{x}}_{max}}$. The maximal entropy was estimated from 100,000 samples drawn from uniform distributions that span the genotype or phenotype space (derivation in Appendix F). Maximal entropies of parameter and phenotype spaces were found to be $H^{\boldsymbol{\theta}}_{max} = 46.979$ and $H^{\boldsymbol{x}}_{max} = 96.037$, respectively. The maximal entropy of the genotype space is found to be lower than that of the phenotype space despite more than a two-fold increase in the number of dimensions. The higher maximal entropy of the phenotype space is caused by significantly larger ranges in all phenotypic dimensions.

2.3 Robustness and evolvability in the GP map

To study the trends in robustness and evolvability around the GP map, the 15-dimensional phenotype space spanning 4 standard deviations around the mean was sampled using a Sobol sequence, a quasi-random generator that results in a more even coverage of the space than random uniform sampling [39]. While the pyloric range spans two standard deviations, four were taken for a holistic view of the GP map which would capture nearly all potential behaviors assuming that the traits are normally distributed. 2,048 Sobol samples were drawn in the phenotype space (Figure 2.2, left) and used as the target traits to sample points from their posterior distributions using SBI. The robustness of each target trait (phenotype) was calculated as the entropy of the resulting posterior distribution of parameters (genotype) (Figure 2.2, middle). For each target trait, the posterior samples in parameter space were then used to simulate the STG model to yield a distribution in phenotype space. The evolvability of the original target traits were then quantified as entropy of these distributions in phenotype space (Figure 2.2, right). The same procedure was done with two standard deviations of range and 1,024 Sobol points to examine robustness and evolvability within the pyloric window.

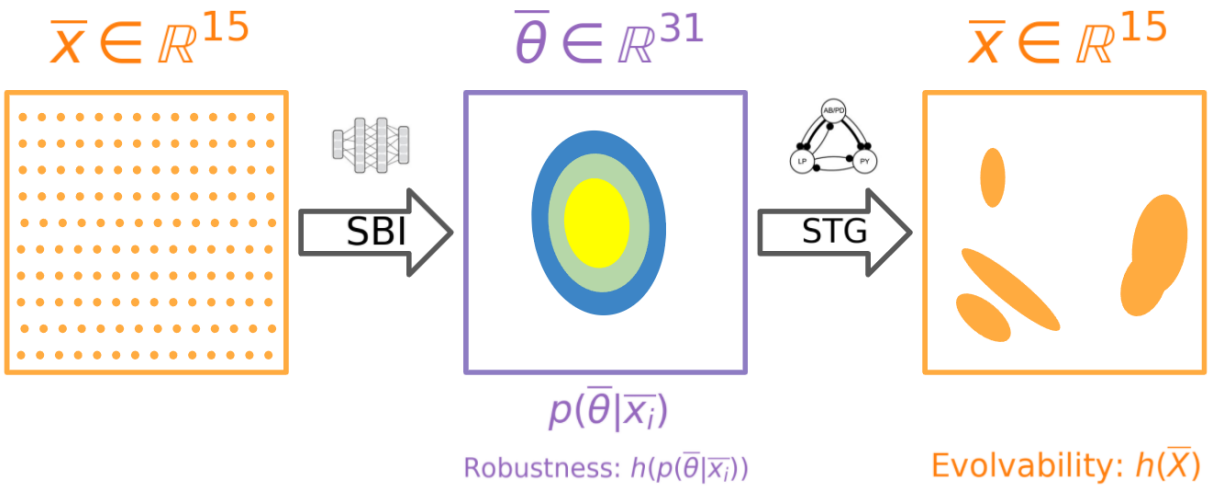

Figure 2.2: Schematic of investigating robustness and evolvability in the GP map. Posterior distributions (middle) of Sobol-distributed points (left) are drawn using SBI. The points are then used to simulate the STG circuit, resulting in a distribution of behaviors arising from the parameter combinations (right). The entropy of the posterior distributions and the resulting phenotype distributions are quantified as robustness and evolvability, respectively.

Filtering invalid behavior While many points in parameter space simply do not map to a phenotype leading to invalid mapping, some resulting phenotype traits are found to be biologically impossible. These phenotypes are excluded from all analyses. The criteria for omission are: 1) the sum of burst durations of all three neurons exceeds cycle period, and 2) any burst durations are negative.

2.4 Structure of the GP map and canalization

To holistically examine the structure of the GP map and possible supported behaviors, the GP map was thoroughly charted using Sobol-generated points as centers for Gaussian sampling [39]. First, the covariance matrix of the posterior distribution of the pyloric rhythm is found to be used as an estimate of mutational step size. Then, 4,096 Sobol-generated points are drawn in the parameter space. These Sobol-generated points are then used as centers for Gaussians with the same covariance as the posterior distribution of the pyloric rhythm. 50,000 samples were drawn from each Gaussian (Figure 2.3, left). The use of Gaussian sampling around Sobol-distributed points produces a a comprehensive coverage of the GP map with 4,096 sets of 50,000 parameter samples. These sets of 50,000 parameter combinations were used to simulate the STG circuit, yielding 4,096 distributions of phenotypes. Canalization was calculated as the inverse of the entropy of these phenotype distributions in each set (Figure 2.3, right).

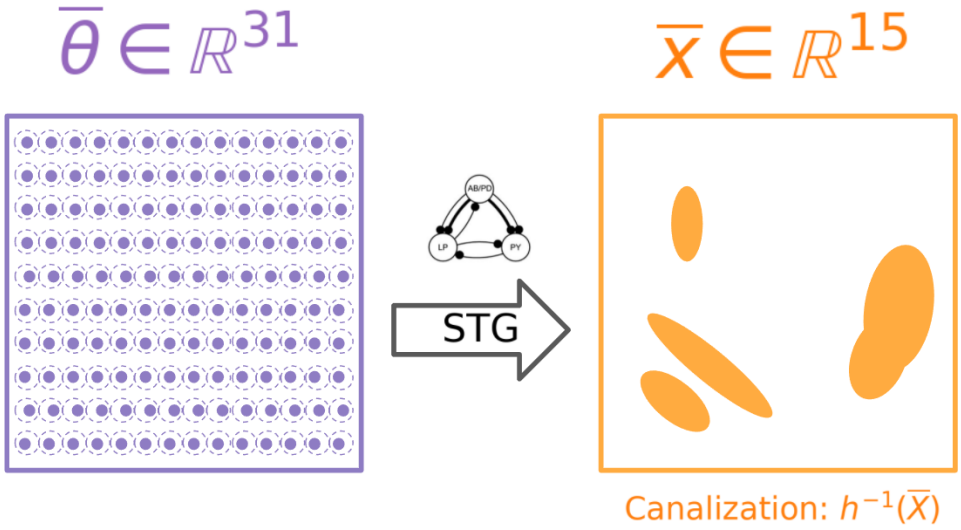

Figure 2.3: Schematic for charting the GP map. Gaussian samples seeded from Sobol-distributed points in parameter space (left) are used to simulate the STG circuit. The resulting phenotype distribution (right) is then quantified to yield an explicit measure of canalization.

This approach is distinct from what is described in Section 2.3 to study robustness and evolvability by studying the local topology of the GP map directly without consideration of any target phenotype. As shown in Figure 2.2, the posterior distributions of a given trait describes a particular region of the parameter space relevant to that specific trait. This skews the interpretation of the GP map towards the given trait. On the other hand, this approach shown in Figure 2.3, samples equal portions of the genotype space that result in varying degrees of phenotypic variation. Effectively, this is equivalent to the visualization in Figure 1.2 in higher dimensions. We take equal portions of the genotype space (Δg, Figure 1.2), and study the phenotypic variation (Δp, Figure 1.2) stemming from this fixed genotypic variation which is given by the covariance of the Gaussian in this instance. Ultimately, this approach unveils the local topology of the GP map around the Sobol-generated points, which evenly represents the GP map.

Chapter 3

Results

3.1 Relationship between robustness and evolvability

No global trend between robustness and evolvability

We first examine the global relationship between robustness and evolvability in the pyloric circuit. The base assumption is that robustness and evolvability are negatively correlated in general due to their intrinsic conflict despite some models showing positive correlation. Figure 3.1 shows the distribution of phenotypic robustness and evolvability found as described in Section 2.3 where each point indicates a Sobol-generated phenotype. No evident trend can be seen between robustness and evolvability among the samples across the GP map. If they were either positively or negatively correlated, clear linear trends with positive or negative slopes, respectively, would be seen. However, this distribution indicates that robustness and evolvability in this neural circuit are not directly related globally as seen in other systems. Rather, a balance between robustness and evolvability seems to be favored in the system as indicated by the grouping of phenotypes around robustness and evolvability values of roughly 0.8. The marginal distributions also show that the points are grouped around the point with robustness and evolability roughly at 0.8. Ultimately, we find that there is no global relationship between robustness and evolvability in the pyloric circuit.

Linearity of robustness and evolvability

Initial investigation failed to identify a direct global relationship between robustness and evolvability in the pyloric rhythm. We hypothesize that the global balance of robustness and evolvability arises from local trends of robustness and evolvability at the level of individual traits. Linear regression was performed on robustness and evolvability of Sobol-generated traits to examine if any particular traits were indicative of either robustness or

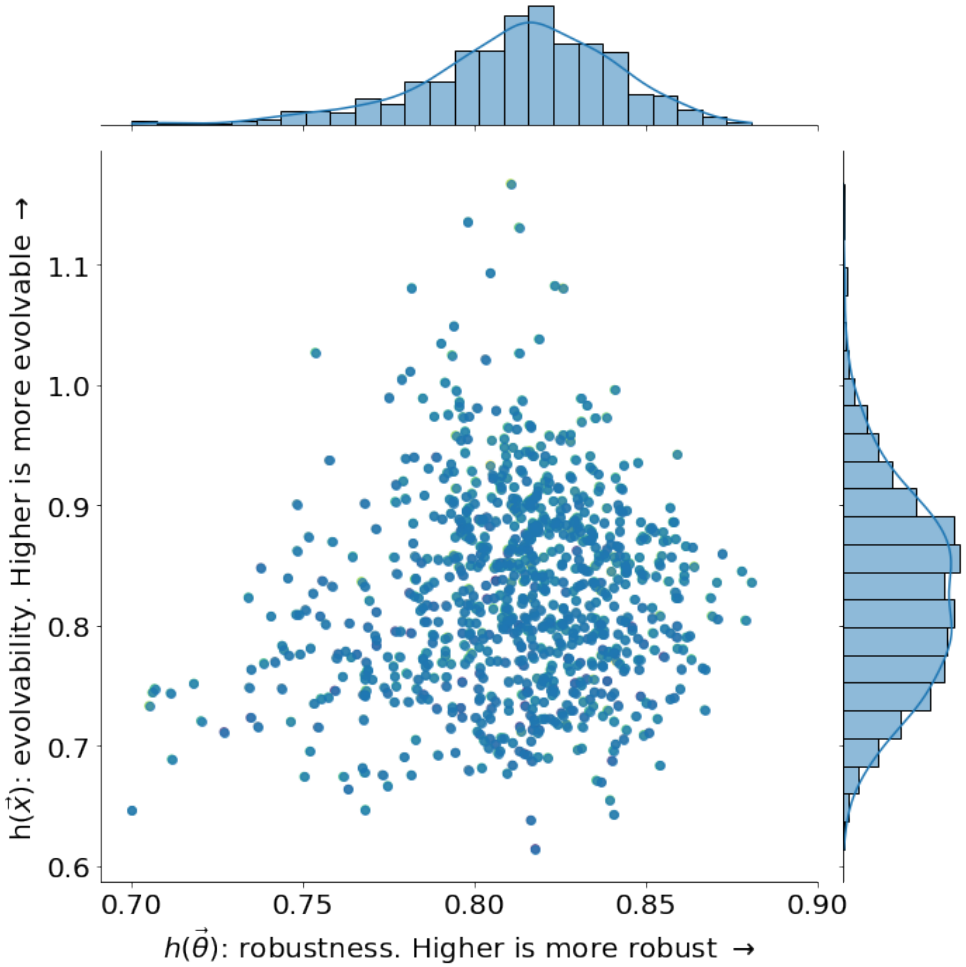

Figure 3.1: Distribution of normalized phenotypic robustness and evolvability. Each dot represents a Sobol-generated point in phenotype space. ($r = 0.09, p = 0.006$)

evolvability. Linear regression was performed using all 15 traits after standardization to reduce the effects of varying orders of magnitude among traits.

Figure 3.2 shows how robustness (purple) and evolvability (orange) in the network depend on individual traits. No clear anti-correlations are seen in most traits. Most traits behave linearly and are coherent to varying degrees in slopes of robustness and evolvability whether they increase or are kept at the same level. On the contrary, the phase gap AB/PD end to LP start, $\Delta\phi_{AB-LP}$, seems to show clearly opposing slopes. These opposing slopes indicate relative importance of this phase gap where this particular trait heavily modulates the final behavior by compensating for deviations in the rhythm caused by other parameters.

Both robustness and evolvability clearly increase with cycle period, T (top left corner). Since cycle period is an overarching trait that defines the rhythmic window, longer period could be a foundation to support more diverse intra-rhythm behaviors, leading to increased

evolvability. The increased number of data points for longer period also indicates that a larger variety of rhythms can be accommodated in longer cycle periods. Increased robustness could also be facilitated by longer cycle periods as the flexibility to deviate while maintaining the characteristic triphasic rhythm increases.

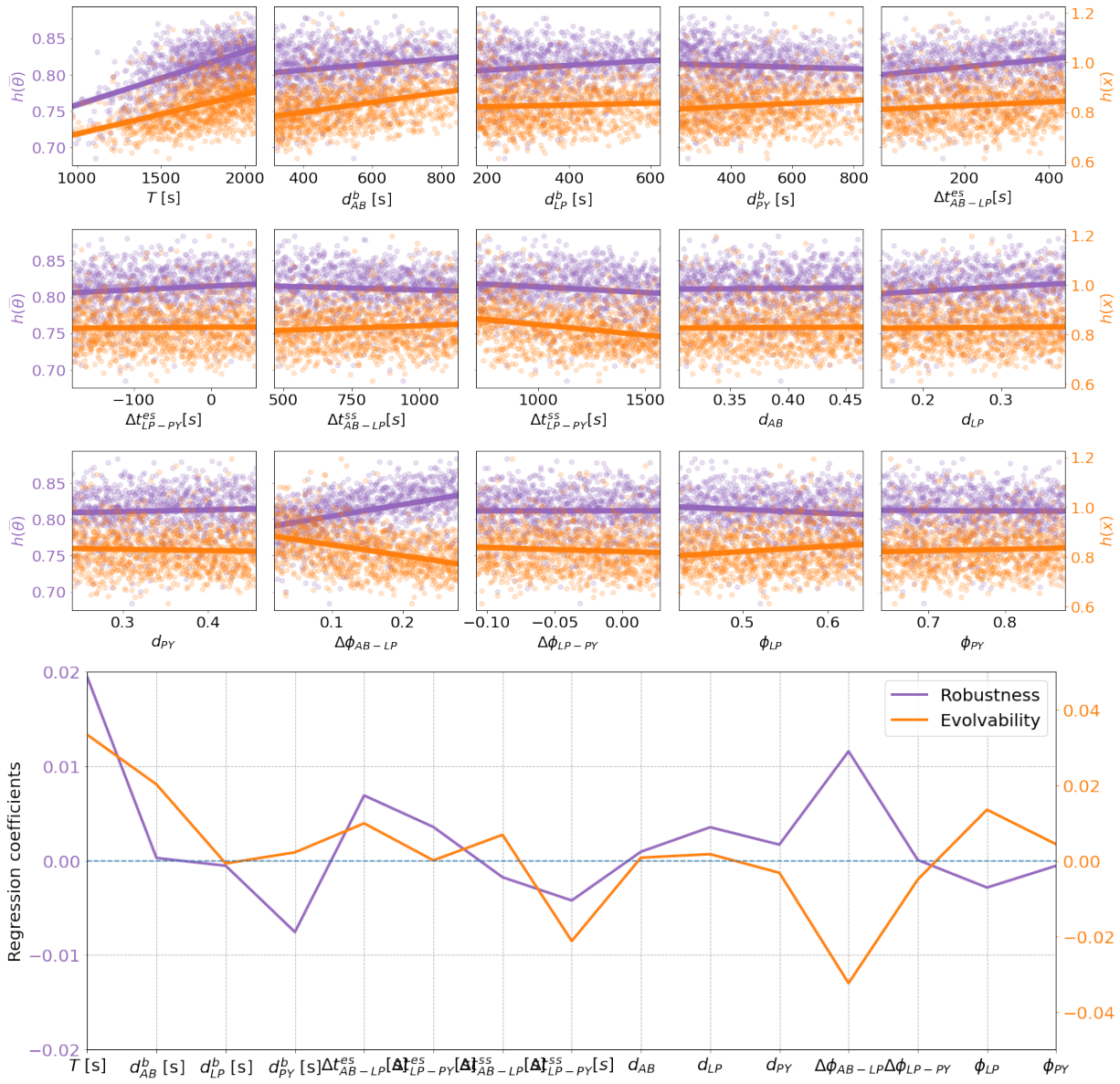

Figure 3.2: (upper) Normalized robustness and evolvability per trait of the pyloric rhythm. Each dot represents a Sobol-generated point (phenotype), and the lines indicate linear fits. r- and p-values of the fits can be found in Appendix A. (lower) Slopes from linear regression of robustness and evolvability using the full 15 phenotypic traits.

Stemming from the predominantly linear trends in robustness and evolvability across the traits, we investigate the linearity of the global robustness and evolvability. Here, we use the linear regression of robustness and evolvability on the full 15 traits. The slopes from linear regression per trait are shown in the lower plot of Figure 3.2. Analogous to the trends per trait, the majority of the coefficients are small in magnitude, and no overall trend can be found over the entirety of the 15-trait vector. Cycle period and phase gap are again the most distinct, reinforcing their importance in modulating the pyloric rhythm. The results coincide qualitatively when looking at phenotypes generated within the pyloric range. These trait-specific trends of robustness and evolvability suggest that most traits have minor contributions to global relationship of robustness and evolvability. However, certain key traits show more notable behavior that hints at their impact in determining the global relationship between robustness and evolvability.

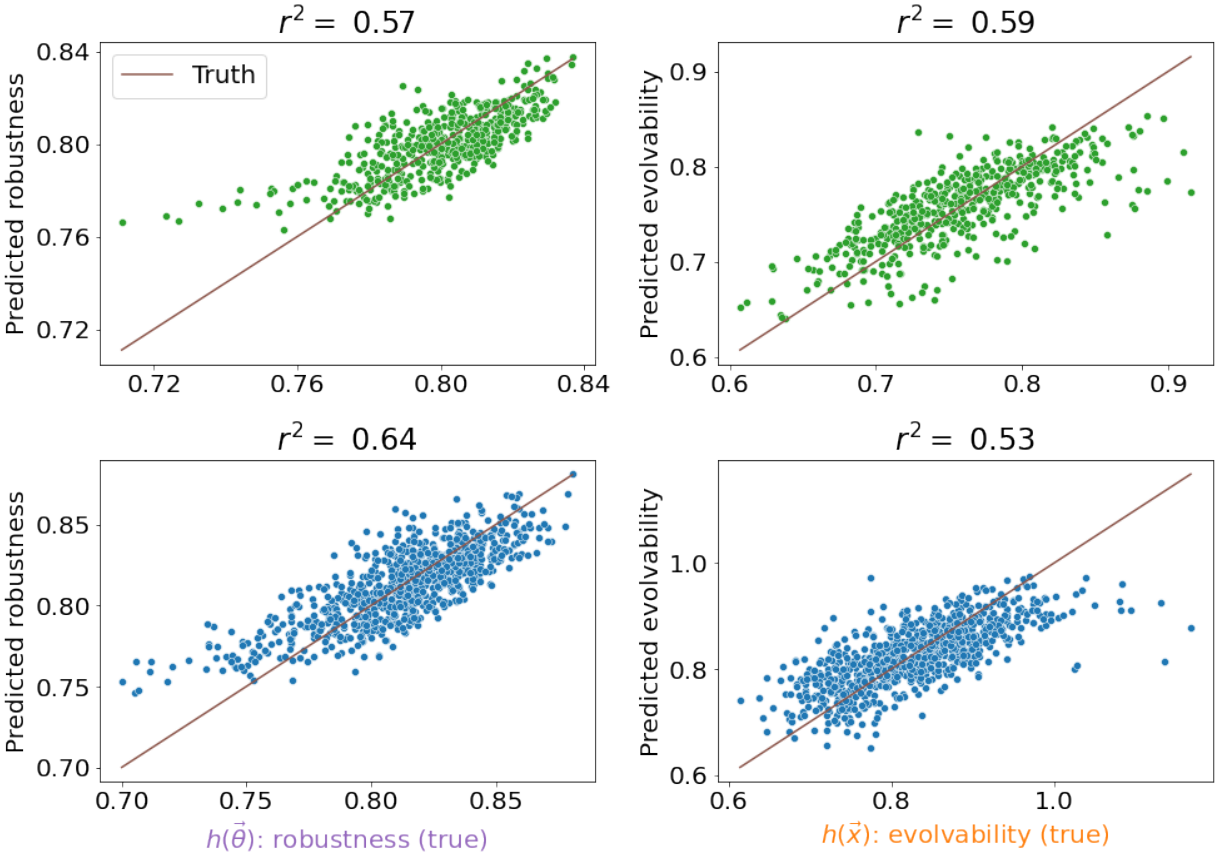

Figure 3.3: Linear regression predictions of robustness (left) and evolvability (right) for the pyloric range ($\mu \pm 2\sigma$; top) and extended range ($\mu \pm 4\sigma$; bottom). The brown lines indicate perfect prediction.

We now examine the regression performances to investigate the global behavior of robustness and evolvability with phenotype. Figure 3.3 shows the predictions from the linear

regression for robustness (left) and evolvability (right) for both pyloric ($\mu \pm 2\sigma$; top) and extended ranges ($\mu \pm 4\sigma$; bottom). The linear fits successfully capture the dominating trends of robustness and evolvability. With all of the r^2 values above 0.53, global robustness and evolvability are largely linear with respect to the pyloric rhythm traits. The global linearity further supports the idea that robustness and evolvability at individual scales aggregate to determine the global trends.

However, there are systemic errors indicated by consistent deviations near the extreme values. For example, the robustness in the pyloric window tends to diverge from the prediction with decreasing robustness. These deviations indicate nonlinear behavior with decreasing robustness and hint at a lower bound of robustness for pyloric rhythms. A lower bound would signify that the pyloric rhythm is produced only when a certain level of robustness can be achieved, possibly to protect the rhythm from small perturbations. Similarly, the asymptotic increase of evolvability for the extended range (bottom right) hints an upper limit for producing novel behavior. An upper limit of evolvability indicates that even a large neutral network is limited to a certain number of accessible phenotypes.

3.2 Canalization around the pyloric rhythm

Robustness and evolvability indicate canalization

We have found that robustness and evolvability are not correlated globally but that they are distributed around a specific point that balances robustness and evolvability. We further see that robustness and evolvability are globally linear with respect to the pyloric rhythm traits which arise from combinations of linear trends of robustness and evolvability at the level of individual traits. Furthermore, we see systemic limits of robustness and evolvability. We hypothesize that the pyloric rhythm is canalized in the GP map that promotes local robustness near pyloric points but evolvability away from pyloric points.

Using the same data shown in Section 2.3, we examine the behavior of robustness and evolability as a function of distance from the pyloric rhythm mean in phenotype space (as shown in Table 1.1). Since the pyloric rhythm is the natural biological behavior that the circuit evolved to produce, we assume that the circuit should be optimized to robustly produce the pyloric rhythm. Figure 3.4 shows robustness and evolvability for Sobol-points sampled within the pyloric (left) and the extended (right) ranges (see Section 2.3). The lower plots show the changes in variance of points grouped in x-axis slices.

The two different ranges show that the pyloric rhythm is a robust optimum. In both ranges, evolvability tends to increase with distance. This increasing evolvability signifies a systemic aim to rapidly explore the GP map to discover an optimum when not near an optimum. The notion of exploring the parameter space in search of a viable optimum of the GP map is aided by increasing variability of evolvability and robustness in both ranges. Canalization requires that the GP map evolves to tightly regulate target behaviors

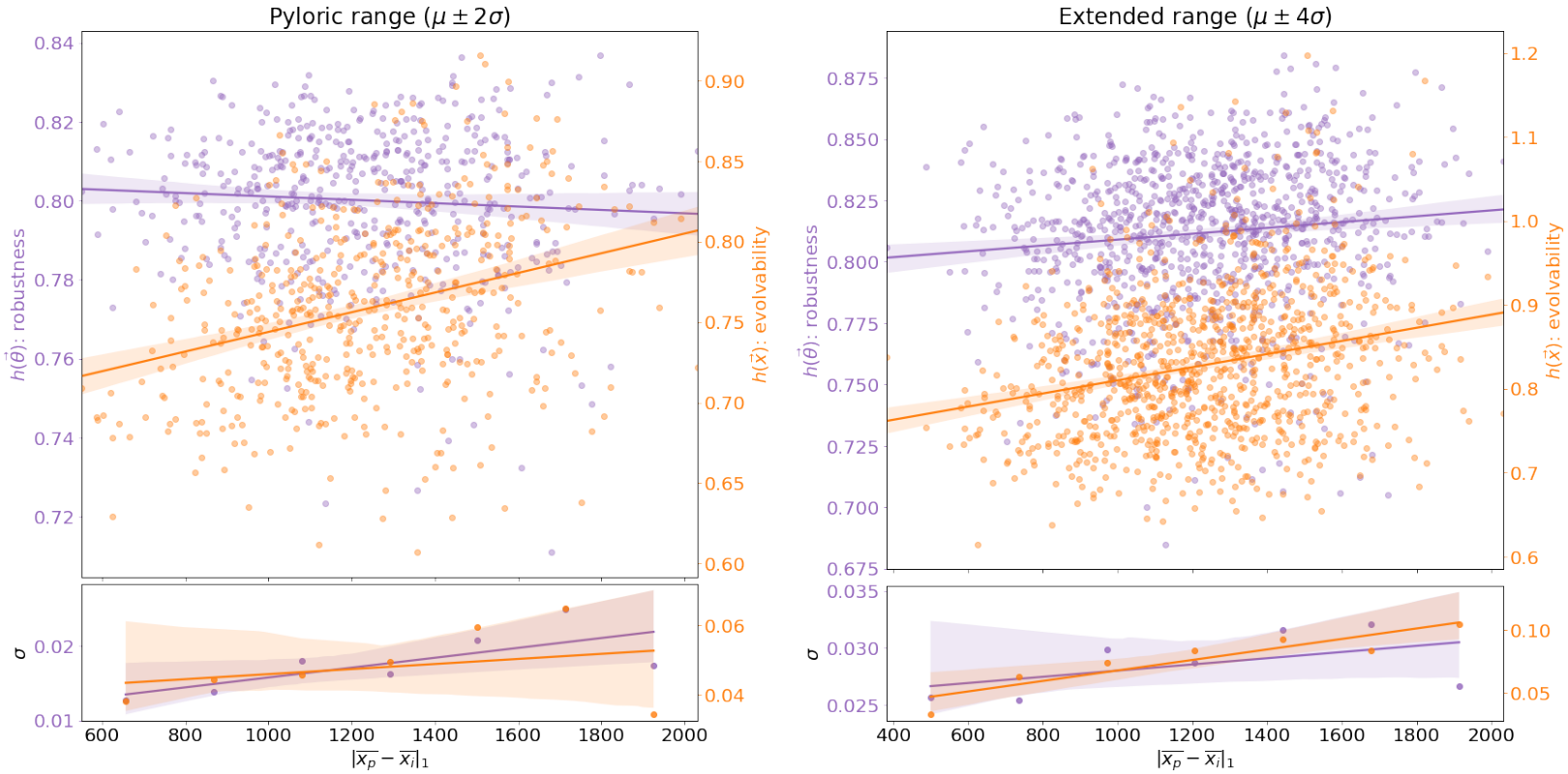

Figure 3.4: (upper) Trends in normalized phenotypic robustness and evolvability with in relation to distance from the mean of the pyloric rhythm, the biological behavior of the system. (lower) The standard deviations of the distribution of points in x-slices for both robustness and evolvability. Left plots show points within the pyloric range ($\mu \pm 2\sigma$) while the right plots show points in the extended range ($\mu \pm 4\sigma$) according to Table 1.1. r- and p-values of the fits of robustness and evolvability in the upper plot can be found in Appendix A.

which naturally forms a uniform and flat topology in the landscape. However, deviating from such areas removes the constraints that canalize behaviors. The lack of constraints allows more variety in the structure of the GP map, resulting in increased variabilities in robustness and evolvability. Both the increasing evolvability and increasing variabilities are corollaries of canalization and support the hypothesis that the pyloric rhythm is canalized.

In the narrower, pyloric range, robustness decreases with distance. This behavior suggests that the pyloric rhythm is maximally robust to parameter perturbations locally within the pyloric range. Contrary to the pyloric range, robustness in the extended range is seen to increase. Given the slight decreasing trend in the pyloric range, the concurrent increase of robustness and evolvability in the extended range could be driven by larger neutral networks. Likewise to increasing variability, moving away from canalized region removes constraints and gives access to increasingly diverse landscapes of the GP map.

Pyloric rhythm is canalized in the GP map

Deviations from linear behavior at lower values of robustness, increasing robustness with distance, along with increasing variabilities for robustness and evolvability with distance all indicate that the pyloric rhythm is canalized. We now directly examine canalization in the GP map to confirm that the pyloric rhythm is indeed canalized. Canalization is calculated following the method described in Section 2.4. The resulting values of canalization as a function of distance to the pyloric posterior mean in the parameter space are shown in upper plot in Figure 3.5. The plot shows that canalization clearly decreases with distance from the pyloric posterior mean. The negative slope directly shows that canalizing behavior exists and that the degree of canalization increases closer to the pyloric rhythm.

The lower part of Figure 3.5 shows a histogram of Gaussian sample sets that yielded no phenotype after simulation. In other words, these samples were drawn from neighborhoods of invalid mapping where none of the parameter combinations leads to behavior. It can be seen that there are no invalid mappings close to the pyloric posterior mean, suggesting that the regions of the GP map around the biological behavior are well-behaved.

We now verify that the observed canalization is specific to the biologically evolved behavior, the pyloric rhythm, and not merely a consequence of a fortunate reference point. To this end, random points were generated in the parameter space to serve as the reference point instead of the pyloric posterior mean. The trends of canalization in relation to the random reference points were found as shown in upper Figure 3.5. A linear fit was done on the distribution of canalization, and canalization score was calculated as the negative of the regression slope. This canalization score describes the trend in canalization with distance to the reference point. A high canalization score indicates that canalization is more drastic around the reference point. Negative canalization score indicates that the reference point is not canalized; that is, canalization can be seen to increase away from the reference point. The canalization scores are shown in Figure 3.6 as a function of distance from randomly generated points to the pyloric posterior mean in parameter space.

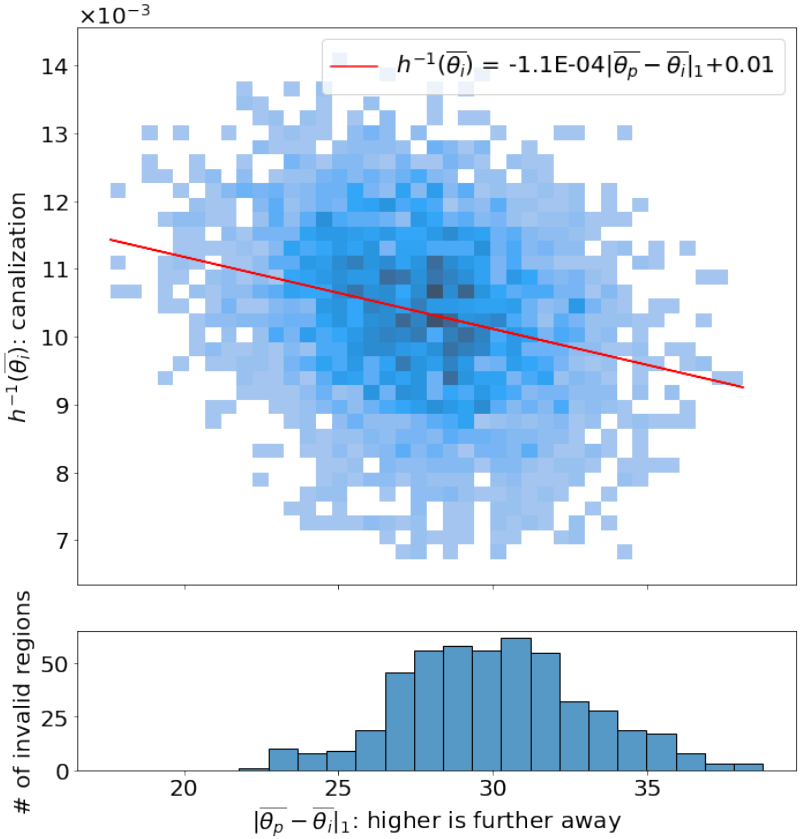

Figure 3.5: (upper) Canalization as a function of distances in parameter space. Red line shows a linear fit where decreasing slope indicates less canalization as distance increases ($r = -0.26, p < 2 \times 10^{-56}$). (lower) Number of Gaussian sampling sets that did not result in any behavior after simulation.

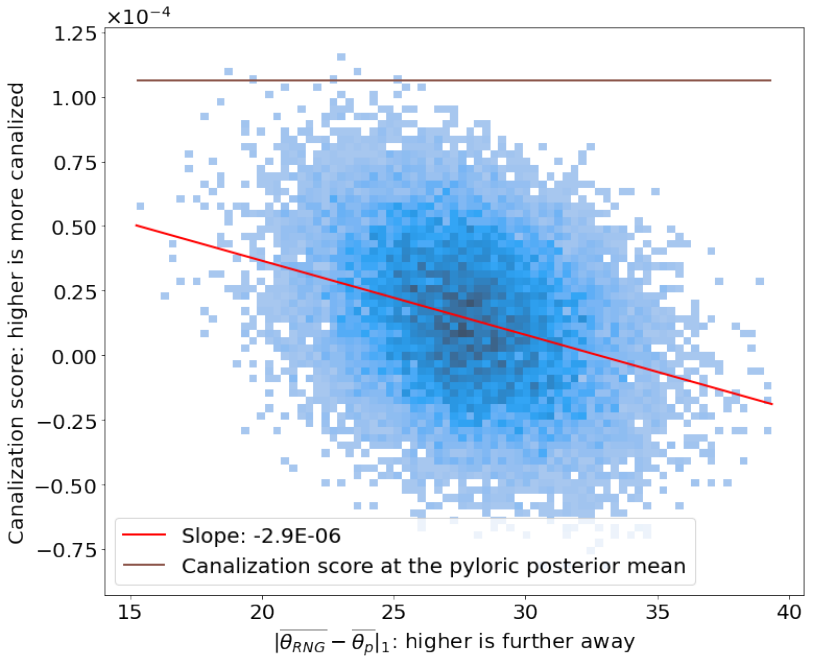

Figure 3.6: Distribution of canalization scores for randomly generated, non-pyloric references points in the parameter space. Red line indicates a linear fit of this data ($r = -0.31, p = 0.0$), and the brown line indicates the canalization score of the pyloric rhythm as a reference.

Canalization score clearly decreases with distance between the randomly generated reference point and the pyloric posterior mean. This decreasing trend shows that the extent of canalizing behavior decreases with increasing disparity in parameters to the pyloric behavior. In addition, the canalization score at the pyloric posterior mean can be seen act as an upper limit with some exceptions. These exceptions could stem from taking the reference point of the pyloric rhythm in the parameter space as the mean of the 31-dimensional posterior distribution. The high dimensionality as well as non-standard shape of the distribution could cause some randomly generated points in the parameter space to overlap with the canalized region. This hypothesis is further supported by the lack of exceptional points at significantly further distances from the pyloric posterior mean. These assessments confirm that canalization is specific to the pyloric rhythm.

Analysis of canalization as shown in Figure 3.5 was also done using the log-likelihood of the random point on the posterior of the mean pyloric rhythm as the distance metric. The results are in qualitative agreement (Appendix C). The log-likelihood as a distance measure gives a more formally accurate understanding as the neutral region in the parameter space is not isotropic around the posterior mean. Testing against randomly generated reference points as in Figure 3.6 was not done as a randomly generated point in parameter space lack a posterior distribution that can be used to calculate likelihood of canalization points.

Properties of the GP map reveal canalizing mechanisms

We next aim to understand how the GP map exhibits canalizing behavior. We hypothesize that the local topology of the GP map enables canalization with flatter regions around the pyloric points promoting robustness. To examine the topology of the GP map, we extensively chart the GP map as described in Section 2.4.

We first look at the log-likelihood, $\ell(\boldsymbol{\theta}; \boldsymbol{x_p})$, of all sampled points in genotype space on the posterior of the pyloric rhythm, $\boldsymbol{x_p}$, to verify that pyloric points lie in regions of high likelihood. As expected, pyloric points score significantly higher compared to the wide range found from non-pyloric points shown in Figure 3.7. While this result seems trivial, it hints at the distribution and possible network of pyloric points in regards to the posterior. Since there is a large discrepancy in sample sizes for pyloric and non-pyloric points, the significance of these distributions were verified by over- and under-sampling (Figure E.1).

To characterize local topology that may give rise to canalization, gradients of the GP map, $\partial\ell(\boldsymbol{\theta}; \boldsymbol{x_p})/\partial\theta_i$, were calculated at each of the sampled points with respect to the parameters. We assume that our sampling method involving Gaussians around Sobol-generated points (see Section 2.4) thoroughly cover the GP map resulting in a comprehensive assessment of GP map gradients. We expect that the gradient magnitudes at pyloric points are more constrained than those at non-pyloric points. In addition, gradients at pyloric points are expected to have smaller magnitude, signifying flatter region of the GP map with higher robustness. Greater gradient magnitude would indicate a steep region in the GP map where genotypic variation results in a large deviation of phenotype from the pyloric rhythm.

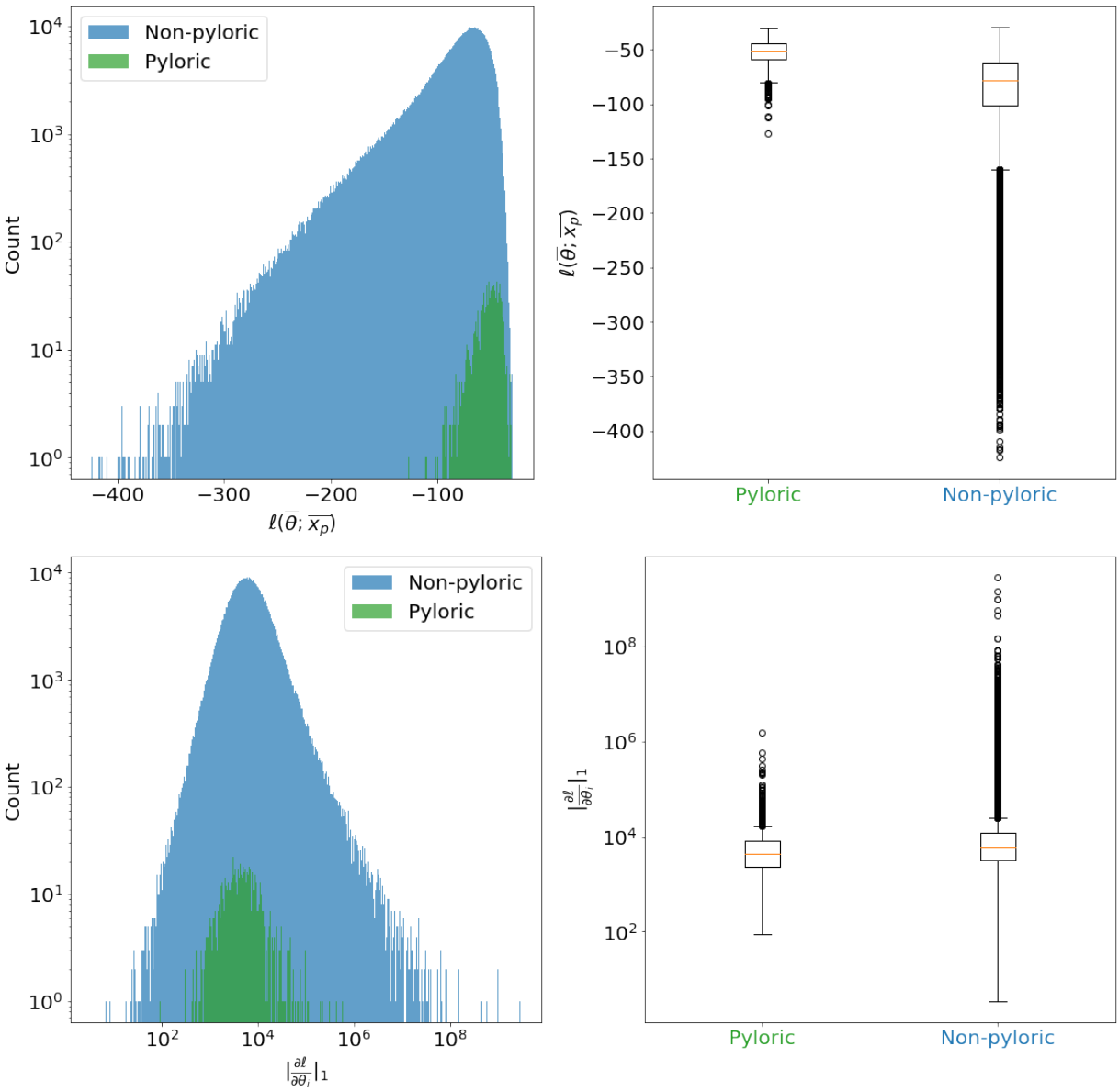

Figure 3.7: (upper) Distribution of log-likelihoods of pyloric and non-pyloric points on the posterior of the pyloric rhythm. (lower) Magnitude of the gradient vector evaluated at pyloric and non-pyloric points. These plots reflect the true sample sizes of pyloric and non-pyloric points, and under- and over-sampled comparisons for verification can be found in Appendix E.

The magnitudes of the gradients for pyloric and non-pyloric points are shown in the lower Figure 3.7. The average gradient magnitudes for both pyloric and non-pyloric are very similar. However, the variance in the magnitudes is much larger for non-pyloric rhythms,

indicating that the local topology around the pyloric points is more uniform and constrained. The large proportion of non-pyloric points with similar gradient magnitudes as pyloric points suggests that the GP map has one or more significant regions that are moderately inclined. Potential for substantial phenotypic change seems to only exist for non-pyloric points as evident by a number of gradient magnitudes that are multiple orders of magnitude higher than the average.

The statistical significance of gradient magnitude distributions were also verified by over- and under-sampling and are shown in Figure E.2. In these sampling, the average gradient magnitudes for pyloric and non-pyloric points are still identical. However, both under- and over-sampling results in higher variance in gradient magnitudes at pyloric points. This result rejects the hypothesis that canalization arises from constrained gradient magnitudes of the GP map at pyloric points. Since neither the average nor the variance of gradient magnitude differ between pyloric and non-pyloric points, the gradient magnitude itself cannot explain how the GP map evolves to canalize the pyloric rhythm.

We still suspect that the topology of the GP map including its gradient enables canalization. We now hypothesize that specific gradient directions shared among pyloric points allow canalization. To test this hypothesis, we calculate the correlation between gradient components across gradients at pyloric points and non-pyloric points separately.

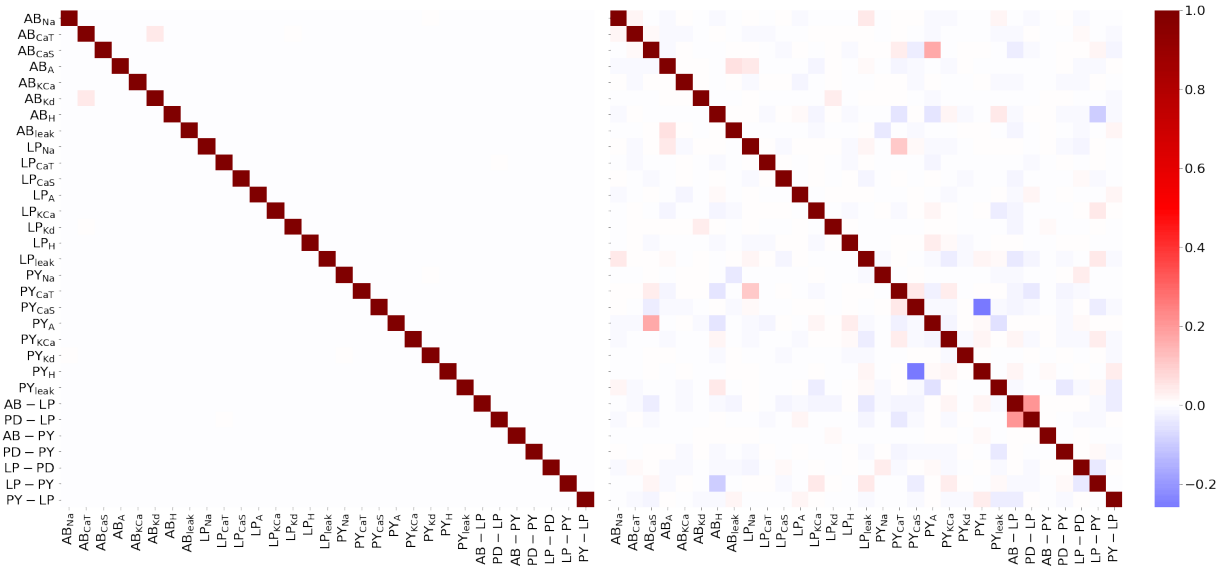

Figure 3.8: Correlation matrices of gradient directions for non-pyloric (left) and pyloric (right) points.

Figure 3.8 shows correlation matrices between the gradient directions across (left) non-pyloric and (right) pyloric points. Clearly, there are no apparent correlations between gradient directions at non-pyloric points. On the contrary, few strong correlations as well as a considerable number of weak correlations between gradient directions are found

for gradients at pyloric points. The distribution of correlation coefficients are shown in Figure 3.9.

The lack of correlations in gradient directions for non-pyloric points is unsurprising as no inherent properties are shared among non-pyloric behaviors. The correlations found in gradient directions at pyloric points signify that the local topology of the GP map at various pyloric points are similar. The specific gradient directions with strong correlations likely indicate mutational directions that preserves the traits of the pyloric rhythm. However, these correlations are not conclusive evidence for mechanisms that enable canalization.

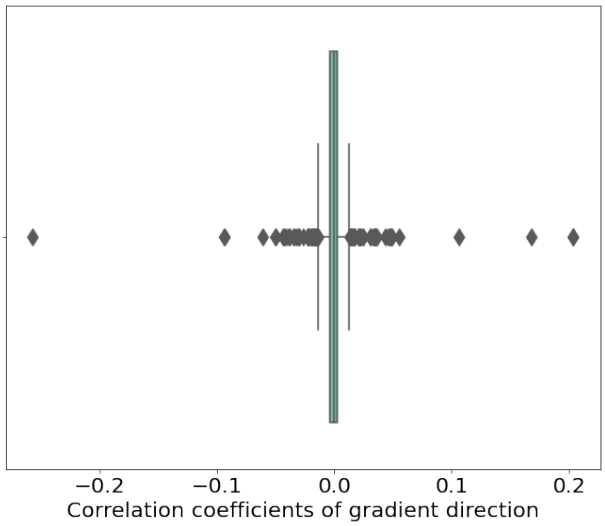

Figure 3.9: Distribution of correlation coefficients between gradient directions at pyloric points as shown in Figure 3.8.

With the gradient direction correlations hinting at a mechanism in GP map gradients to enable canalization, we examine the GP map gradient magnitude as a function of distance to the nearest pyloric point. This approach is similar to that of Figure 3.4 with the difference being that now we examine gradient magnitudes as indicators of robustness and evolvability as opposed to calculated values. Additionally, this approach searches for canalizing behavior in parameter space, not phenotype space. If the GP map gradients are mechanisms of canalization, we expect constraints in gradient magnitudes in close proximity to pyloric points. We can also expect that gradient magnitudes will increase with distance as deviation from canalized areas typically result in greater phenotypic variation.

Figure 3.10 shows that the gradient magnitude increases with distance to the nearest pyloric point in parameter space. This trend reinforces the conclusion that the pyloric rhythm is canalized in the GP map and also supports the idea that the structure of the GP map, its gradients enable canalization.

The gradient magnitude variability is reduced closer to pyloric points, consistent with the behavior seen in robustness and evolvability. Constrained gradient magnitude near the pyloric points support the depiction of the GP map with constrained flat regions in the vicinity of pyloric points that promote robustness, enabling canalization. The gradient magnitude variability otherwise shows quadratic behavior and reach a maximal variance before decreasing. The quadratic trend in variance shows that the robust flat areas are followed by a large diversity of gradient landscapes resulting from lack of constraints in the GP map and high dimensionality of the system. Ultimately, the landscape becomes

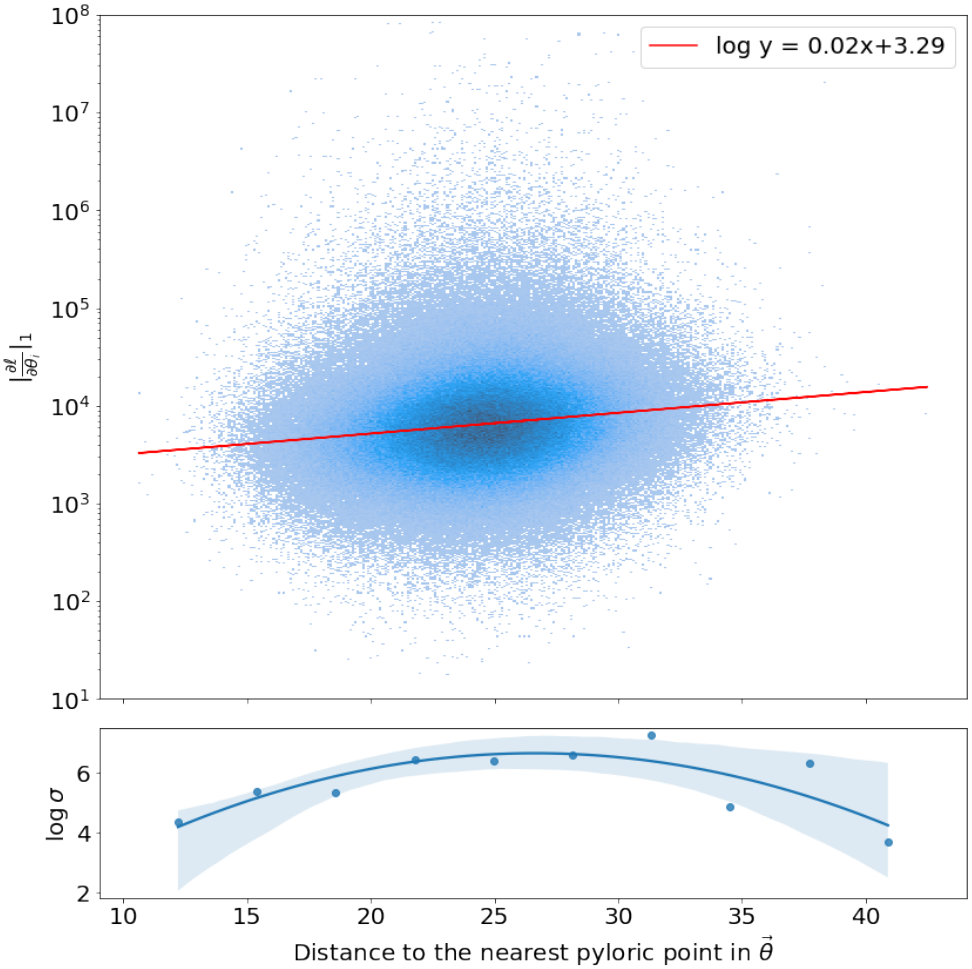

Figure 3.10: (upper) Distribution of gradient magnitudes with respect to their distances to the nearest pyloric point in parameter space. Red line indicates a linear fit ($r = 0.14, p = 0.0$). (lower) Log of standard deviations of magnitudes in x-slices. Blue line indicates a quadratic fit.

less varied, possibly due to the map not being defined beyond a certain region or the lack of samples at such great distances.

Chapter 4

Discussion and Outlook

This work aimed to study the relationship between two evolutionary properties, robustness and evolvability. By employing information theoretic and analytical approaches as well as a novel simulation-based technique, we quantified robustness and evolvability in a model neural network and characterized their relationship across the genotype-phenotype map. While a straightforward relationship does not exist between robustness and evolvability in the pyloric circuit, we found that they are linear with respect to individual traits as well collectively. Additionally, we found that the network balances robustness and evolvability around a point in the GP map. Thus, we hypothesize that robustness and evolvability in this neural network are promoted by canalization around the pyloric rhythm, the biological behavior that the GP map evolved to exhibit.

We found evidence of canalization in trends of robustness and evolvability away from the pyloric point, and calculating canalization around the GP map confirmed that the pyloric point is canalized. We then searched for mechanisms that facilitate canalization in the topology of the GP map. The hypothesis that gradient magnitudes at pyloric points will be smaller was disproved, but examining the correlations of gradient directions revealed possible implicit mechanisms of the GP map at pyloric points that could preserve the pyloric rhythm. Finally, looking at gradient magnitudes as a function of distance to the nearest pyloric point showed identical behaviors to robustness and evolvability in relation to distance to the pyloric rhythm mean. Robustness and evolvability are distinct indicators of demonstrated canalization, which illuminates gradients of the GP map as promoter of canalization.

Ultimately, the relationship between robustness and evolvability in the pyloric circuit was not found to be direct as in other systems [6, 7]. A particular evolutionary effect, canalization, was identified which elucidated the relationship between robustness and evolvability in the pyloric network. We find that the pyloric rhythm is canalized as a consequence of the topology of the GP map. These results suggest that evolutionary properties in complex systems such as neural circuits require consideration of the underlying GP map to fully understand their behaviors and driving mechanisms.

Potential combination of this investigation with biological phylogenetic data can reveal potentially relevant structures in the GP map that can replicate evolution over time. For example, phylogenetic knowledge of a speciation event can be used to recreate the genetic and phenotypic structures at those time points. The subsequent evolution of biological behavior can then be modeled to progress concurrently as mutational trajectories in the GP map. These studies could also potentially answer dynamics of evolutionary change such as punctuated equilibrium.

The STG pyloric circuit used in this study exhibits one characteristic rhythm and is thus simple in both model and behavior. The existence of a single behavioral optimum has potential simplifying effects on the GP map. However, many neural systems are more complex and exhibit a diversity of behaviors. The cricket's song recognition network, for example, has multiple behavioral preferences, and hence applying the basis of this study to more complex systems could yield more dynamic structures in the GP map such as multiple canalized optima.

Additionally, while the individual traits of the rhythmic phenotype were not the focus of this work, examination into the details of the STG model would be necessary to explain the various behaviors of traits and their relative importance at the model level. Understanding specific compensatory mechanisms in the neural circuit should be the basis for explicit knowledge of parameter interactions for any specific model.

Further investigation into the structure that embeds pyloric points in the genotype space could yield insight into a possible neutral network structure within the system that can further aid in the understanding of evolutionary properties (See Appendix B). Examination of the underlying network structure can also uncover mutational potential around the GP map (see Appendix D). This will give explicit information on potential phenotypes through mutation as well as possible mutational trajectories around the GP map.

Finally, the methods used in this work can be applied generally to any system involving a mechanistic model. Various simulation-based inference techniques allow accurate and efficient posterior estimation in higher dimensional space. Information entropy as a measure for robustness and evolvability can be applied to any discrete or continuous system and can easily be scaled to any number of dimensions. Considering the GP map as an analog to phenotype landscapes allows compelling mathematical analysis involving multiple genetic interactions, of which only a select few were used in this work [9]. These developments in theory and method set the foundation for future studies of evolutionary properties in complex biological systems.

Acknowledgements

First and foremost I would like to thank Jan for the opportunity to work on this project and the continual support throughout the process. I am incredibly grateful to be introduced to such an interesting topic in such a supportive environment.

I would like to thank Victor for his valuable feedback and positive support not only in this thesis work but also during my studies in Lund.

I would also like to thank the members of the Neural Computation and Behavior lab at ENI who have been very welcoming and helpful during my time at the lab.

This work used the Scientific Compute Cluster at GWDG, the joint data center of Max Planck Society for the Advancement of Science (MPG) and University of Göttingen.

Bibliography

[1] Ellen M. Leffler et al. "Revisiting an Old Riddle: What Determines Genetic Diversity Levels within Species?" In: *PLOS Biology* 10.9 (Sept. 11, 2012), e1001388. ISSN: 1545-7885. DOI: 10.1371/journal.pbio.1001388. URL: https://journals.plos.org/plosbiology/article?id=10.1371/journal.pbio.1001388 (visited on 12/27/2021).

[2] Erik M. Rauch and Yaneer Bar-Yam. "Theory Predicts the Uneven Distribution of Genetic Diversity within Species". In: *Nature* 431.7007 (7007 Sept. 2004), pp. 449–452. ISSN: 1476-4687. DOI: 10.1038/nature02745. URL: https://www.nature.com/articles/nature02745 (visited on 12/27/2021).

[3] Thomas F. Hansen. "The Evolution of Genetic Architecture". In: *Annual Review of Ecology, Evolution, and Systematics* 37.1 (2006). Examples of different evolvability systems.
Discussion on pleitropy and epistasis, pp. 123–157. DOI: 10.1146/annurev.ecolsys.37.091305.110224. URL: https://doi.org/10.1146/annurev.ecolsys.37.091305.110224 (visited on 08/23/2021).

[4] Thomas F Hansen. "Is Modularity Necessary for Evolvability?: Remarks on the Relationship between Pleiotropy and Evolvability". In: *Biosystems* 69.2 (May 1, 2003). More genes affecting a trait -> more evolvable
Evolvability: ability to respond to directional selection, pp. 83–94. ISSN: 0303-2647. DOI: 10.1016/S0303-2647(02)00132-6. URL: https://www.sciencedirect.com/science/article/pii/S0303264702001326 (visited on 08/30/2021).

[5] Stephen Jay Gould and Niles Eldredge. "Punctuated Equilibria: The Tempo and Mode of Evolution Reconsidered". In: *Paleobiology* 3.2 (1977), pp. 115–151. ISSN: 0094-8373. JSTOR: 2400177.

[6] Andreas Wagner. "Robustness and Evolvability: A Paradox Resolved". In: *Proceedings of the Royal Society B: Biological Sciences* 275.1630 (Jan. 7, 2008), pp. 91–100. DOI: 10.1098/rspb.2007.1137. URL: https://royalsocietypublishing.org/doi/full/10.1098/rspb.2007.1137 (visited on 09/29/2021).

[7] Christine Mayer and Thomas F. Hansen. "Evolvability and Robustness: A Paradox Restored". In: *Journal of Theoretical Biology* 430 (Oct. 7, 2017). Thesis in file.

Continuous case using activator-inhibitor model, pp. 78–85. ISSN: 0022-5193. DOI: 10.1016/j.jtbi.2017.07.004. URL: https://www.sciencedirect.com/science/article/pii/S0022519317303296 (visited on 05/11/2021).

[8] James M. Whitacre. "Degeneracy: A Link between Evolvability, Robustness and Complexity in Biological Systems". In: *Theor Biol Med Model* 7.1 (Feb. 18, 2010). Degeneracy leads to increased robustness as opposed to redundancy.
Support of other statements. Robustness is a prerequisite for complexity., p. 6. ISSN: 1742-4682. DOI: 10.1186/1742-4682-7-6. URL: https://doi.org/10.1186/1742-4682-7-6 (visited on 05/11/2021).

[9] Sean H. Rice. "The Evolution of Canalization and the Breaking of Von Baer's Laws: Modeling the Evolution of Development with Epistasis". In: *Evolution* 52.3 (1998). GP MAP
mathematical expression of canalization -> evolvability
Divergence for speciation to find new optima
Large shift in optimum can lead to increased variance which can lead to divergence, pp. 647–656. ISSN: 1558-5646. DOI: 10.1111/j.1558-5646.1998.tb03690.x. URL: https://onlinelibrary.wiley.com/doi/abs/10.1111/j.1558-5646.1998.tb03690.x (visited on 09/09/2021).

[10] C. H. Waddington. *The Strategy of the Genes*. Routledge, Apr. 29, 2014. 275 pp. ISBN: 978-1-317-65755-2. Google Books: 69l1AwAAQBAJ.

[11] Stephen C. Stearns. "Progress on Canalization". In: *PNAS* 99.16 (Aug. 6, 2002), pp. 10229–10230. ISSN: 0027-8424, 1091-6490. DOI: 10.1073/pnas.172388999. pmid: 12149521. URL: https://www.pnas.org/content/99/16/10229 (visited on 01/11/2022).

[12] Suzanne L. Rutherford and Susan Lindquist. "Hsp90 as a Capacitor for Morphological Evolution". In: *Nature* 396.6709 (6709 Nov. 1998), pp. 336–342. ISSN: 1476-4687. DOI: 10.1038/24550. URL: https://www.nature.com/articles/24550 (visited on 01/13/2022).

[13] Christine Queitsch, Todd A. Sangster, and Susan Lindquist. "Hsp90 as a Capacitor of Phenotypic Variation". In: *Nature* 417.6889 (6889 June 2002), pp. 618–624. ISSN: 1476-4687. DOI: 10.1038/nature749. URL: https://www.nature.com/articles/nature749 (visited on 01/13/2022).

[14] Benjamin H. White. "What Genetic Model Organisms Offer the Study of Behavior and Neural Circuits". In: *J Neurogenet* 30.2 (June 2016), pp. 54–61. ISSN: 0167-7063. DOI: 10.1080/01677063.2016.1177049. pmid: 27328841. URL: https://www.ncbi.nlm.nih.gov/pmc/articles/PMC6336385/ (visited on 01/09/2022).

[15] Jan Clemens et al. "A Small, Computationally Flexible Network Produces the Phenotypic Diversity of Song Recognition in Crickets". In: *eLife* 10 (Nov. 11, 2021). Ed. by Ronald L Calabrese, e61475. ISSN: 2050-084X. DOI: 10.7554/eLife.61475. URL: https://doi.org/10.7554/eLife.61475 (visited on 11/16/2021).

[16] Kyle Cranmer, Johann Brehmer, and Gilles Louppe. "The Frontier of Simulation-Based Inference". In: *PNAS* 117.48 (Dec. 1, 2020), pp. 30055–30062. ISSN: 0027-8424, 1091-6490. DOI: 10.1073/pnas.1912789117. pmid: 32471948. URL: https://www.pnas.org/content/117/48/30055 (visited on 01/09/2022).

[17] Pedro J Gonçalves et al. "Training Deep Neural Density Estimators to Identify Mechanistic Models of Neural Dynamics". In: *eLife* 9 (Sept. 17, 2020). Ed. by John R Huguenard, Timothy O'Leary, and Mark S Goldman, e56261. ISSN: 2050-084X. DOI: 10.7554/eLife.56261. URL: https://doi.org/10.7554/eLife.56261 (visited on 12/20/2021).

[18] Tamra C. Mendelson and Kerry L. Shaw. "Rapid Speciation in an Arthropod". In: *Nature* 433.7024 (7024 Jan. 2005), pp. 375–376. ISSN: 1476-4687. DOI: 10.1038/433375a. URL: https://www.nature.com/articles/433375a (visited on 01/09/2022).

[19] T. Blankers, A. K. Lübke, and R. M. Hennig. "Phenotypic Variation and Covariation Indicate High Evolvability of Acoustic Communication in Crickets". In: *Journal of Evolutionary Biology* 28.9 (2015), pp. 1656–1669. ISSN: 1420-9101. DOI: 10.1111/jeb.12686. URL: https://onlinelibrary.wiley.com/doi/abs/10.1111/jeb.12686 (visited on 01/09/2022).

[20] Astrid A. Prinz, Dirk Bucher, and Eve Marder. "Similar Network Activity from Disparate Circuit Parameters". In: *Nat Neurosci* 7.12 (12 Dec. 2004), pp. 1345–1352. ISSN: 1546-1726. DOI: 10.1038/nn1352. URL: https://www.nature.com/articles/nn1352 (visited on 08/09/2021).

[21] Gabrielle J. Gutierrez, Timothy O'Leary, and Eve Marder. "Multiple Mechanisms Switch an Electrically Coupled, Synaptically Inhibited Neuron between Competing Rhythmic Oscillators". In: *Neuron* 77.5 (Mar. 6, 2013), pp. 845–858. ISSN: 0896-6273. DOI: 10.1016/j.neuron.2013.01.016. URL: https://www.sciencedirect.com/science/article/pii/S0896627313000822 (visited on 01/09/2022).

[22] Mark S. Goldman et al. "Global Structure, Robustness, and Modulation of Neuronal Models". In: *J. Neurosci.* 21.14 (July 15, 2001), pp. 5229–5238. ISSN: 0270-6474, 1529-2401. DOI: 10.1523/JNEUROSCI.21-14-05229.2001. pmid: 11438598. URL: https://www.jneurosci.org/content/21/14/5229 (visited on 09/20/2021).

[23] Jacob Ratliff et al. "Neuronal Oscillator Robustness to Multiple Global Perturbations". In: *Biophysical Journal* 120.8 (Apr. 20, 2021). However, all biochemical reactions are temperature dependent, so every physiological property that underpins neuronal and circuit function will be altered by a temperature change. For this reason, we refer to a temperature perturbation as a global perturbation.
This simple example illustrates why increased variability is expected near a transition point in a dynamical system: ongoing, internal noise perturbations cause variability in the system's dynamics. As the system approaches a transition, its sensitivity generically increases, and the impact of the internal noise becomes more visible.

Robustness to temperature and pH in the environment, pp. 1454–1468. ISSN: 0006-3495. DOI: 10.1016/j.bpj.2021.01.038. URL: https://www.sciencedirect.com/science/article/pii/S0006349521001478 (visited on 09/20/2021).

[24] Eve Marder and Dirk Bucher. "Central Pattern Generators and the Control of Rhythmic Movements". In: *Current Biology* 11.23 (Nov. 27, 2001), R986–R996. ISSN: 0960-9822. DOI: 10.1016/S0960-9822(01)00581-4. URL: https://www.sciencedirect.com/science/article/pii/S0960982201005814 (visited on 12/22/2021).

[25] Allen Selverston. "Stomatogastric Ganglion". In: *Scholarpedia* 3.4 (Apr. 2, 2008). scholarpedia overview, p. 1661. ISSN: 1941-6016. DOI: 10.4249/scholarpedia.1661. URL: http://www.scholarpedia.org/article/Stomatogastric_ganglion (visited on 08/09/2021).

[26] L. F. Abbott and Eve Marder. "Modeling Small Networks". In: *In C Koch and I Segev, Editors, Methods in Neuronal Modelling*. Mit Press, 1998, pp. 361–410.

[27] Lamont S. Tang et al. "Robustness of a Rhythmic Circuit to Short- and Long-Term Temperature Changes". In: *J. Neurosci.* 32.29 (July 18, 2012), pp. 10075–10085. ISSN: 0270-6474, 1529-2401. DOI: 10.1523/JNEUROSCI.1443-12.2012. pmid: 22815521. URL: https://www.jneurosci.org/content/32/29/10075 (visited on 01/30/2022).

[28] David Greenberg, Marcel Nonnenmacher, and Jakob Macke. "Automatic Posterior Transformation for Likelihood-Free Inference". In: *Proceedings of the 36th International Conference on Machine Learning*. International Conference on Machine Learning. PMLR, May 24, 2019, pp. 2404–2414. URL: https://proceedings.mlr.press/v97/greenberg19a.html (visited on 01/16/2022).

[29] George Papamakarios, David Sterratt, and Iain Murray. "Sequential Neural Likelihood: Fast Likelihood-free Inference with Autoregressive Flows". In: *Proceedings of the Twenty-Second International Conference on Artificial Intelligence and Statistics*. The 22nd International Conference on Artificial Intelligence and Statistics. PMLR, Apr. 11, 2019, pp. 837–848. URL: https://proceedings.mlr.press/v89/papamakarios19a.html (visited on 03/02/2022).

[30] C E Shannon. "A Mathematical Theory of Communication". In: (), p. 53.

[31] Andrew Feutrill and Matthew Roughan. "A Review of Shannon and Differential Entropy Rate Estimation". In: *Entropy* 23.8 (8 Aug. 2021), p. 1046. DOI: 10.3390/e23081046. URL: https://www.mdpi.com/1099-4300/23/8/1046 (visited on 09/29/2021).

[32] Günter P. Wagner, Ginger Booth, and Homayoun Bagheri-Chaichian. "A Population Genetic Theory of Canalization". In: *Evolution* 51.2 (1997). mutation reveals variation
Rate of canalization, pp. 329–347. ISSN: 1558-5646. DOI: 10.1111/j.1558-5646.1997.tb02420.x. URL: https://onlinelibrary.wiley.com/doi/abs/10.1111/j.1558-5646.1997.tb02420.x (visited on 12/09/2021).

[33] Vincent Debat and Patrice David. "Mapping Phenotypes: Canalization, Plasticity and Developmental Stability". In: *Trends in Ecology & Evolution* 16.10 (Oct. 1, 2001), pp. 555–561. ISSN: 0169-5347. DOI: 10.1016/S0169-5347(01)02266-2. URL: https://www.sciencedirect.com/science/article/pii/S0169534701022662 (visited on 12/12/2021).

[34] Eve Marder, Marie L Goeritz, and Adriane G Otopalik. "Robust Circuit Rhythms in Small Circuits Arise from Variable Circuit Components and Mechanisms". In: *Current Opinion in Neurobiology*. SI: Brain Rhythms and Dynamic Coordination 31 (Apr. 1, 2015). Degeneracy aids in robustness
Large enough systems have degeneracy, pp. 156–163. ISSN: 0959-4388. DOI: 10.1016/j.conb.2014.10.012. URL: https://www.sciencedirect.com/science/article/pii/S0959438814002128 (visited on 09/20/2021).

[35] *Training Deep Neural Density Estimators to Identify Mechanistic Models of Neural Dynamics*. mackelab, Mar. 12, 2021. URL: https://github.com/mackelab/IdentifyMechanisticModels_2020 (visited on 12/31/2021).

[36] Charu C. Aggarwal, Alexander Hinneburg, and Daniel A. Keim. "On the Surprising Behavior of Distance Metrics in High Dimensional Space". In: *Database Theory — ICDT 2001*. Ed. by Jan Van den Bussche and Victor Vianu. Red. by Gerhard Goos, Juris Hartmanis, and Jan van Leeuwen. Vol. 1973. Lecture Notes in Computer Science. Berlin, Heidelberg: Springer Berlin Heidelberg, 2001, pp. 420–434. ISBN: 978-3-540-41456-8 978-3-540-44503-6. DOI: 10.1007/3-540-44503-X_27. URL: http://link.springer.com/10.1007/3-540-44503-X_27 (visited on 12/06/2021).

[37] Paul Brodersen. *Entropy Estimators*. Dec. 28, 2021. URL: https://github.com/paulbrodersen/entropy_estimators (visited on 12/31/2021).

[38] Alexander Kraskov, Harald Stögbauer, and Peter Grassberger. "Estimating Mutual Information". In: *Phys. Rev. E* 69.6 (June 23, 2004), p. 066138. DOI: 10.1103/PhysRevE.69.066138. URL: https://link.aps.org/doi/10.1103/PhysRevE.69.066138 (visited on 09/29/2021).

[39] Stephen Joe and Frances Y. Kuo. "Constructing Sobol Sequences with Better Two-Dimensional Projections". In: *SIAM J. Sci. Comput.* 30.5 (Jan. 1, 2008), pp. 2635–2654. ISSN: 1064-8275. DOI: 10.1137/070709359. URL: https://epubs.siam.org/doi/10.1137/070709359 (visited on 10/13/2021).

Appendix A

Performance of linear regression

Table A.1: r- and p- values of linear regression per trait shown in upper Figure 3.2.

	Robustness		Evolvability	
	r	p	r	p
T	0.55	0.00	0.46	0.00
d^b_{AB}	0.19	0.00	0.35	0.00
d^b_{LP}	0.13	0.00	0.11	0.002
d^b_{PY}	-0.07	0.04	0.11	0.001
Δt^{es}_{AB-LP}	0.21	0.00	0.13	0.00
Δt^{es}_{LP-PY}	0.12	0.00	0.02	0.51
Δt^{ss}_{AB-LP}	-0.07	0.06	0.07	0.06
Δt^{ss}_{LP-PY}	-0.11	0.002	-0.22	0.00
d_{AB}	0.01	0.77	0.06	0.11
d_{LP}	0.15	0.00	0.02	0.52
d_{PY}	0.04	0.28	-0.03	0.43
$\Delta\phi_{AB-LP}$	0.41	0.00	-0.40	0.00
$\Delta\phi_{LP-PY}$	0.01	0.80	-0.10	0.01
ϕ_{LP}	-0.09	0.01	0.16	0.00
ϕ_{PY}	-0.04	0.28	0.09	0.01

Table A.2: r- and p- values of linear regression per trait shown in upper Figure 3.4

	Robustness		Evolvability	
	r	p	r	p
Pyloric range	-0.06	0.15	0.31	3×10^{-13}
Extended range	0.12	7×10^{-4}	0.27	$1 \times 10^{-}15$

Appendix B

Distribution of pyloric points in genotype space

Figure B.1 (left) shows the distance from one pyloric point to the nearest pyloric point in the parameter space within the generated samples that maps to a valid phenotype. The right plot shows the distribution of all pairwise distances between the pyloric points. Both of these distance distributions are fairly normal and not particularly indicative of the structure of the neutral network.

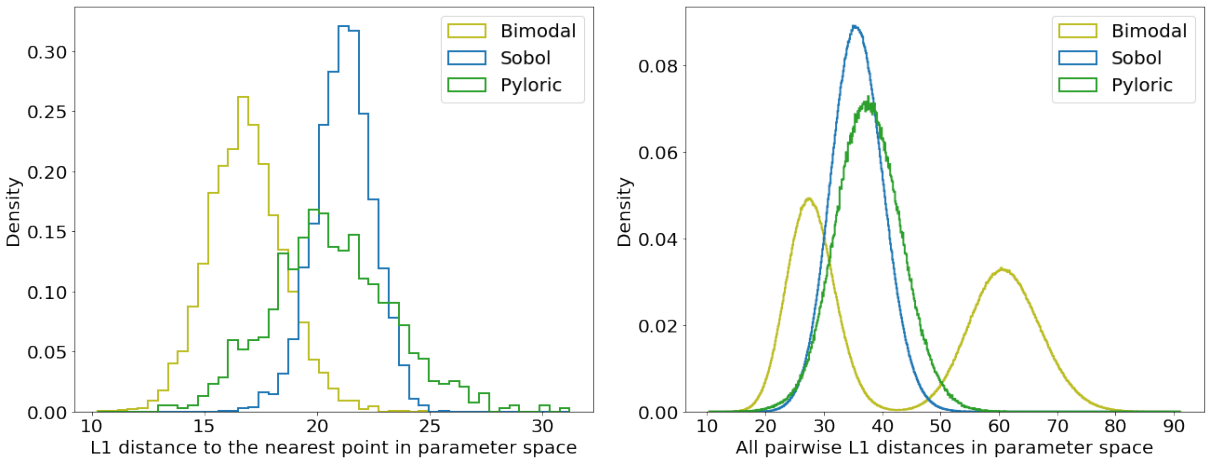

Figure B.1: (left) Distribution of distances in parameter space from one pyloric point to the nearest pyloric point. (right) Distribution of all pairwise distances in parameter space between pyloric points. Sobol indicates a Sobol-generated points intended to represent a uniform grid in parameter space. Bimodal indicates samples generated from two Gaussians centered at opposite ends of the parameter space.

Comparing the distribution of pyloric points to other examples gives a slightly better picture. Sobol-distributed points, representing a uniform grid, and bimodallly distributed

points are also shown in Figure B.1. All pairwise distance of the bimodal distribution can be clearly seen as bimodal while Sobol points are similarly Gaussian with a slightly lower mean. With a lower mean and larger variance in closest distance than Sobol points, the distribution of pyloric points can be thought to be slightly less uniformly distributed around the parameter space, possibly forming sparse clusters.

The distribution of pyloric points among non-pyloric points can be seen in Figure B.2. The vastness of the non-pyloric points effectively shape the bounds of the parameter space, and consistent with Figure B.1, distribution of pyloric points is even throughout the space with higher concentration towards the center. However this method compresses 31 dimensions into two, destroying a large proportion of information and potentially misconstruing the actual distribution.

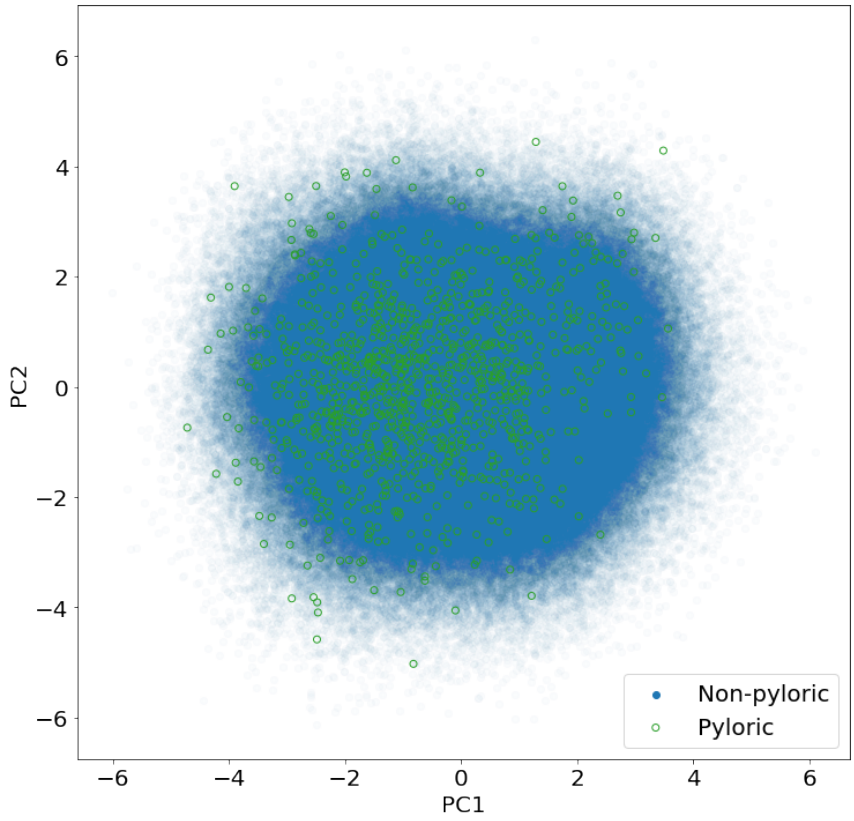

Figure B.2: PCA view of pyloric points (green outline) distributed across the parameter space.

Appendix C

Likelihood as a distance metric

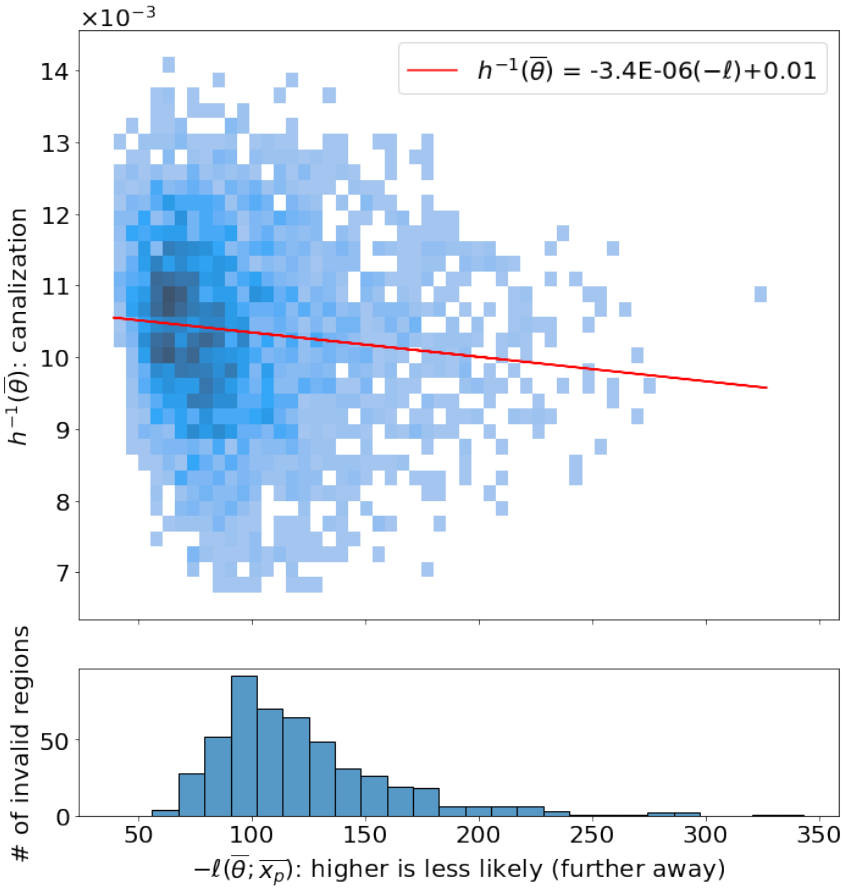

Figure C.1: Canalization shown as a function of likelihood; analogous to Figure 3.5.

Appendix D

Diverse distribution of behaviors in a mutational step

Figure D.1 shows examples of resulting phenotype distributions from Gaussian sampling as discussed in Section 2.4. The pulse and pause durations, understood to be key traits in acoustic communication and rhythmic behavior, are extracted from the firing of a neuron. As evident by the stark differences in the distributions, the local topology of the GP map has significant influence on deviations in parameter space. These distributions directly show the influence of GP map on robustness and evolvability. While the data shown are extracted from one neuron, data from other neurons were qualitatively similar.

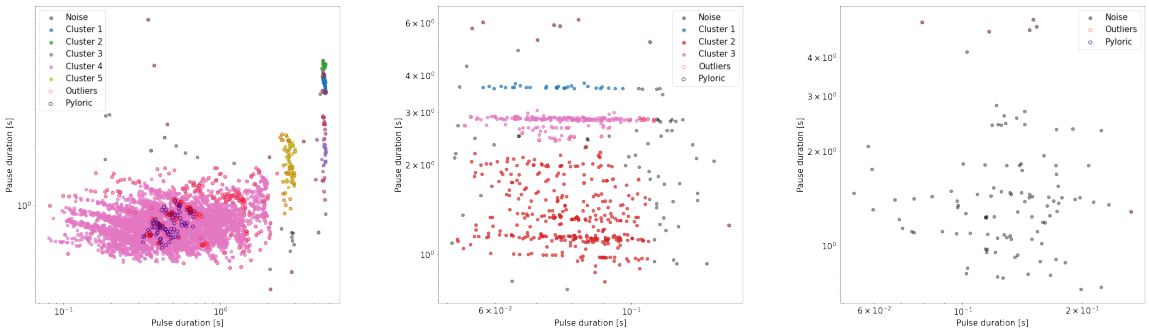

Figure D.1: Diverse range of behaviors arising from same-sized Gaussian sampling on different regions of the GP map.

Appendix E

Over- and under-sampling of likelihood and gradient norm

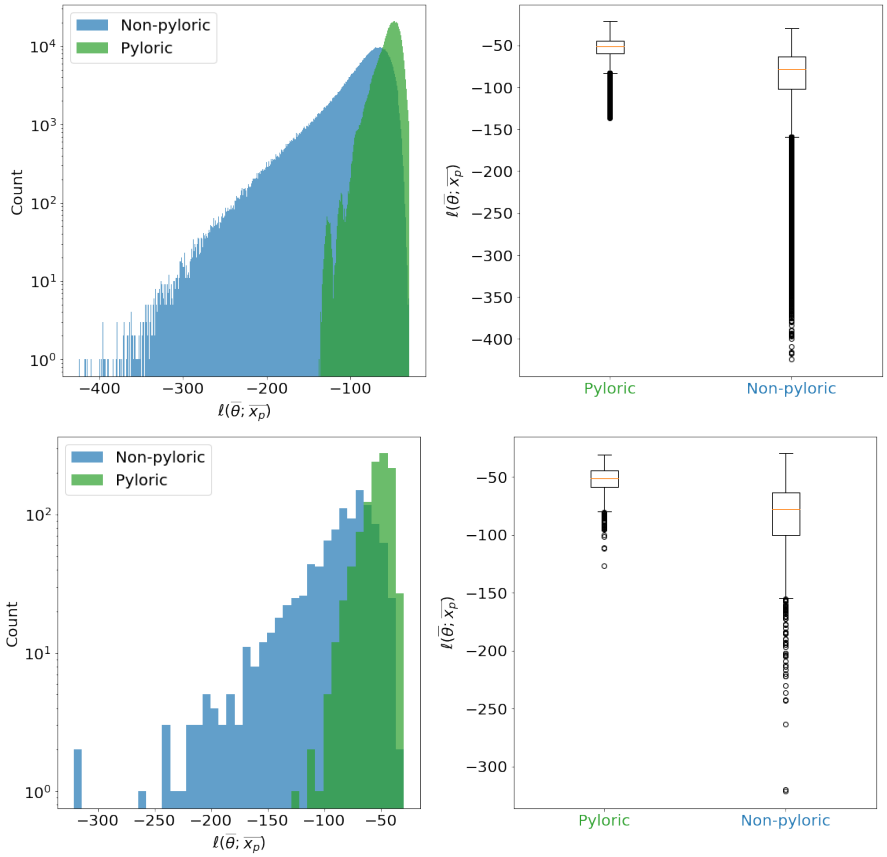

Figure E.1: (top) Pyloric samples were oversampled to match the non-pyloric sample size, and non-pyloric samples were under-sampled to match the pyloric sample size (bottom).

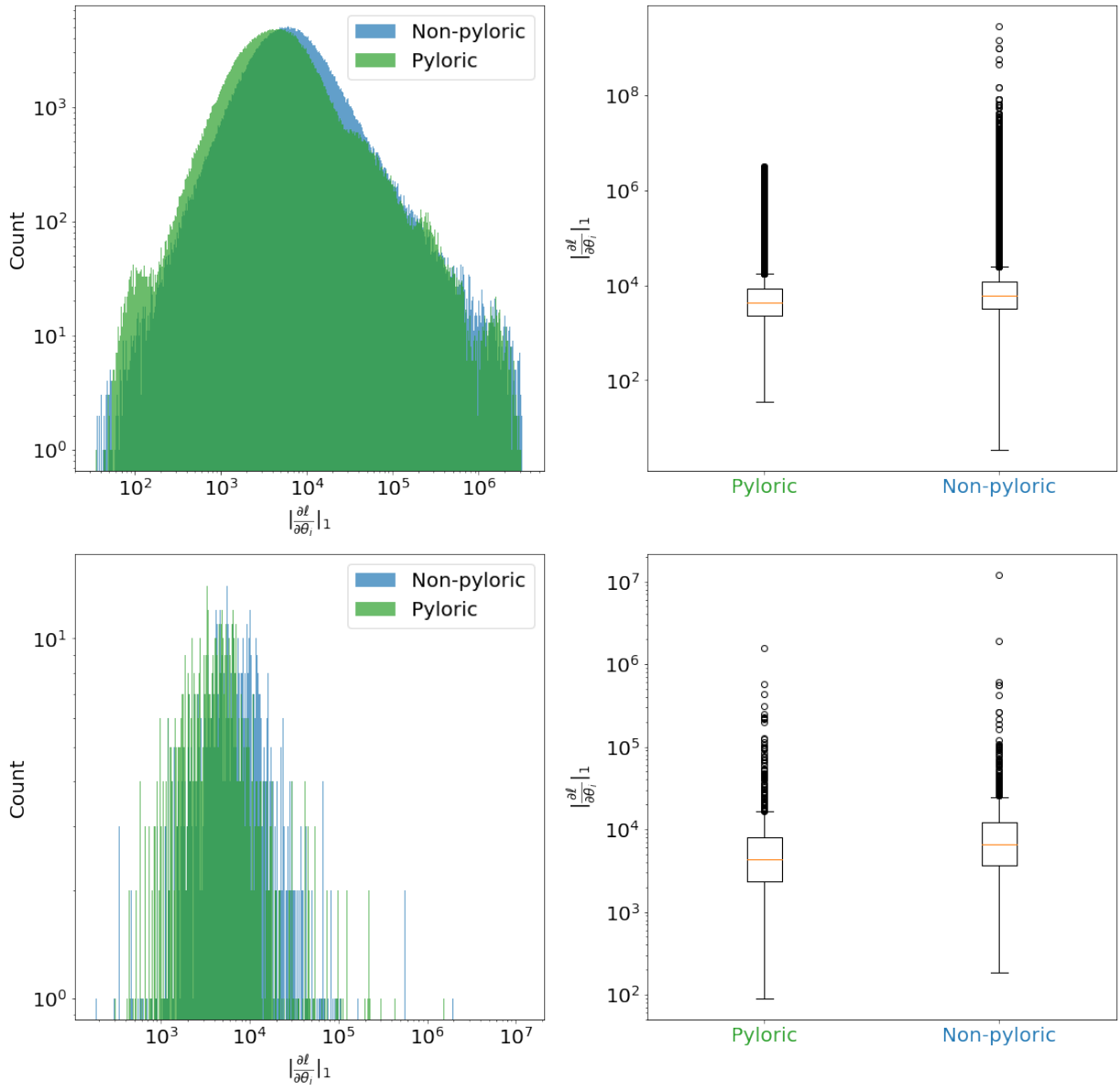

Figure E.2: (top) Pyloric samples were oversampled to match the non-pyloric sample size, and non-pyloric samples were under-sampled to match the pyloric sample size (bottom).

Appendix F

Derivation of maximal entropy

As used in normalization of entropy, the maximum entropy of a bounded space is given by the entropy of a uniform distribution that spans the space. The below derivation shows that for a bounded system with no other constraints, a uniform distribution that spans the entire space has the maximum entropy. While the derivation is of a one-dimensional case, it can be generalized to higher dimensions. Considering a one-dimensional space spanning $[a, b]$, the entropy of a uniform distribution is calculated as

$$H(x) = -\int_a^b p(x) \log p(x) dx \tag{F.1}$$

. Introducing a Lagrange multiplier, λ,

$$\mathcal{L} = -\int_a^b p(x) \log p(x) dx + \lambda \int_a^b p(x) dx - \lambda \tag{F.2}$$

$$\frac{\partial \mathcal{L}}{\partial p(x)} = -1 - \log p(x) + \lambda = 0 \Rightarrow p(x) = \exp(\lambda - 1) \tag{F.3}$$

$$\Rightarrow \int_a^b e^{1-\lambda} dx = 1 \Rightarrow \lambda = 1 - \log\left(\frac{1}{b-a}\right) \tag{F.4}$$

$$p(x) = \exp\left[1 - 1 + \log\left(\frac{1}{b-a}\right)\right] \Rightarrow p(x) = \frac{1}{b-a} \tag{F.5}$$

. Hence the distribution that yields maximal entropy in this space is given by a uniform distribution spanning the domain.